Revision 1 (manuscript 4251)

Redox systematics of martian magmas with implications for magnetite stability

K. Righter[1], L. Danielson[2], K. Pando[2], R.V. Morris[1], T. G. Graff[2], D. G. Agresti[3], A. M. Martin[1], S. Sutton[4,5], M. Newville[5], A. Lanzirotti[5].

[1]NASA/JSC,

[2]ESCG, Houston, TX 77058,

[3]University of Alabama at Birmingham,

[4]Department of Geophysical Sciences and [5]Center for Advanced Radiation Sources, Univ. Chicago.

Submitted 5/31/2012

Revised 10/12/2012

Abstract

Magnetite is commonly found at sites on Mars explored by robotic spacecraft, yet is rare in martian meteorites and in experimental studies of martian magma compositions. Iron redox systematics of the high FeO shergottitic liquids are poorly known, yet have a fundamental control on stability of phases such as magnetite, ilmenite, and pyroxenes. We undertook experiments to constrain the $Fe^{3+}/\Sigma Fe$ in high FeO (15-22 wt%) glasses as a function of fO_2, melt P_2O_5, temperature and pressure. We also performed a series of sub-liquidus experiment between 1100 and 1000 °C and FMQ+0.5 to FMQ-1 to define magnetite stability. Run products were analyzed for Fe^{3+} and Fe^{2+} by Mössbauer spectroscopy and micro-XANES (x-ray absorption near edge structure) spectroscopy. One bar liquids equilibrated at FMQ-3 to FMQ+3 show a much lower $Fe^{3+}/\Sigma Fe$ than terrestrial basalts at the same conditions. As melt P_2O_5 contents increase from 0 to 3 wt.% (at fixed pressure, temperature and fO_2), $Fe^{3+}/\Sigma Fe$ decreases from 0.07 to 0.05, but this is within error on the measurements. Temperature increases between 1200 and 1500 °C cause little to no variation in $Fe^{3+}/\Sigma Fe$. Pressure increases from 1 to 4 GPa cause a 0.06 decrease in $Fe^{3+}/\Sigma Fe$. The trends with pressure and temperature are in agreement with results of previous studies. Combining our new series of data allows derivation of an expression to calculate Fe^{3+}/Fe^{2+} for high FeO melts such as martian magmas.

$$\ln(Fe^{3+}/Fe^{2+}) = = a\ \ln fO_2 + b/T + cP/T + dX_{FeO} + eX_{Al2O3} + fX_{CaO} + gX_{Na2O} + hX_{K2O} + iX_{P2O5}$$

This expression can be used to show that decompressed melts become slightly more oxidized at the surface (compared to 4 GPa). Magnetite stability is suppressed by the lower Fe^{3+}/Fe^{2+} of the high FeO melts. Magnetite stability is a function of Fe_2O_3 and temperature and is stable ~50 °C lower than typical terrestrial basalt. Difficulty in producing magnetite as a liquidus phase in magmatic systems suggests either that many martian basalts are more oxidized than FMQ (but not represented among meteorite collections), that the titano-magnetite only forms upon cooling below ~ 1000 °C at FMQ, or that the magnetite has a secondary origin.

1.0 Introduction

Recent exploration of martian surface mineralogy has revolutionized our understanding of the diversity of minerals present at the surface. In particular, it is clear that magnetite hosts most of the iron in basaltic rocks at Gusev Crater (Morris et al. 2008a). These authors make the reasonable argument that the magnetite is likely primary, based on its chemical composition and parameters derived from Mössbauer spectra. This is, however, inconsistent with: a) the low modal abundance of magnetite in martian meteorites, and b) the current lack of knowledge of iron redox equilibria and phase relationsF in martian magmas. For example, the nakhlites (clinopyroxenites) contain ~1% titanomagnetite as skeletal grains in the mesostasis (Treiman 2005), and basaltic shergottites (pigeonite and plagioclase (maskelynite) bearing basalt) contain 1 to 3.5 % titanomagnetite in the groundmass (e.g., Xirouchakis et al. 2002; Stolper and McSween 1979, Mikouchi 1998); these are relatively small amounts compared with the abundances in many rocks analyzed at Gusev Crater (~10 %). Phase equilibria studies of shergottites have not reported abundant magnetite down to temperatures of ~1050 °C at the FMQ buffer (Stolper and McSween 1979; McCoy and Lofgren 1999), whereas in terrestrial basaltic magmas magnetite is stable with abundances between 5 – 10 % at 1050 to 1100 °C. In fact, the only published 1 bar experiments to stabilize magnetite are those at higher fO_2 - FMQ+4 (McCoy and Lofgren 1999), and at higher pressures with water dissolved in the magma (Minitti and Rutherford 2000; Dann et al. 2001). Furthermore, in terrestrial basalts magnetite stability is strongly influenced by fO_2 and magnetite is stable at 1150 °C at FMQ+2, and as low as 1070 °C at FMQ-1 (**Figure 1**). This dependence on fO_2 is not predicted for shergottites such as Los Angeles, which has a magnetite field at low temperatures, but is apparently not fO_2-dependent

(Xirouchakis et al. 2002). However, the latter predictions are based on the MELTS algorithm that is calibrated using terrestrial magma compositions.

Attempts to examine this problem from the perspective of $Fe^{3+}/\Sigma Fe$ (defined as $Fe^{3+}/(Fe^{3+}+Fe^{2+})$) ratio in silicate melts, which should control magnetite stability, are hampered by the lack of data on $Fe^{3+}/\Sigma Fe$ for relatively FeO-rich and Al_2O_3-poor shergottite-like compositions (**Figure 2**). There are also no data for P_2O_5-bearing basaltic melts (like the shergottites) that can contain up to 3 wt% P_2O_5. Existing data for $Fe^{3+}/\Sigma Fe$ in melts are dominated by compositions within the terrestrial basalt and andesite fields (Kress and Carmichael 1991; Sack et al. 1980; Kilinc et al. 1983). Of the few existing data for high FeO shergottitic melt compositions, some have low (below 0.1) $Fe^{3+}/\Sigma Fe$ compared to values in terrestrial systems of well over 0.2 at similar oxygen fugacities (Morris et al. 2008a), whereas others are higher (McCanta et al. 2004; **Fig. 3**). There is also some hint of non-linear dependence of $Fe^{3+}/\Sigma Fe$ as FeO is increased in a given melt composition (Jayasuriya et al. 2004).

These lines of evidence suggest that the Fe redox systematics of martian magmas are not fully understood, including the factors controlling the saturation of a martian magma with magnetite. Our understanding of the variation of Fe^{3+} and Fe^{2+} in martian magmas is incomplete and deserves some attention. We report here the initial results of a systematic approach to understanding 1) iron redox equilibria as a function of melt composition (P_2O_5), temperature, fO_2, pressure and H_2O, and 2) phase equilibria of shergottites to investigate magnetite stability. With this combination, the seemingly conflicting $Fe^{3+}/\Sigma Fe$ results of McCanta et al. (2004) and Morris et al. (2008a) (higher and lower, respectively, than predicted values), can be addressed, as well as the question of whether there is a critical $Fe^{3+}/\Sigma Fe$ required for magnetite stability, and if so, at what temperature, pressure and fO_2.

2.0 Experimental techniques:

Two synthetic basaltic shergottite compositions, one similar to the bulk composition of Zagami (sherg 1; Table 1) and the other more MgO-rich (sherg 6; Table 1), were prepared from high purity oxides and homogenized by repeated fusion and grinding. Some experiments (series A and C) were carried out at 1 bar in gas-mixing furnaces with fO_2 controlled by CO-CO_2 mixtures (Table 2). Samples were held in the hot spot of the furnace using Re wire loops. High pressure experiments (Series B) were carried out in piston cylinder and multi-anvil apparatuses at NASA-JSC (Righter et al. 2008; 2009; Table 2).

Series A: This series was carried out at 1 bar between FMQ–3 and FMQ+3 at 1250 ºC and constrains the variation of $Fe^{3+}/\Sigma Fe$ for a martian basaltic melt over a large fO_2 range. Three additional compositions were prepared with variable P_2O_5 contents to explore the effect of P_2O_5 at the FMQ buffer. Oxygen fugacity of interest was achieved by CO-CO_2 gas mixtures. Experiments were held at superliquidus temperatures for 3 days and then drop-quenched into water.

Series B: These experiments were designed to define the effect of pressure on the $Fe^{3+}/\Sigma Fe$ in the shergottite, and were carried out at higher pressures in piston cylinder (following the approach of Righter et al. 2009) and multi-anvil apparatuses. Multi-anvil experiments were carried out in the COMPRES G2 assembly (Figure 4) (Leinenweber et al. 2012). Pressure calibration was achieved using the quartz-coesite transition at 1000 °C (Bose and Ganguly 1995), the fayalite-gamma spinel transition at 1200 °C (Yagi et al. 1987), and the majorite-perovskite transition of $CaGeO_3$ at 1000 °C (Ross et al. 1986). Phases were identified using Raman spectroscopy of polished samples. Sample pressure was determined using a simple linear fit to phase transition data. Multi-anvil experiments were pressurized to 4 GPa, then heated to

1600 °C for 20 minutes, and quenched by shutting off heater power. Some experiments were completed in capsules machined from a solid rod of high purity Mo metal. These experiments buffer fO_2 at the Mo-MoO_2 buffer, near IW (O'Neill 1986). Other experiments were carried out in a graphite capsule, with a pellet of a 50-50 mix of Co metal and CoO and MgO loaded above the capsule. In these experiments, fO_2 is monitored by a Co-(CoMg)O sliding sensor (Taylor et al. 1992) that equilibrated at FMQ-2 (Righter et al. 2009).

Series C: This series was carried out at 1 bar at subliquidus conditions to define magnetite stability. Several experiments were carried out at FMQ-1 and variable temperature (1000 to 1100 °C). Others were carried out at fixed temperature (1050 °C) and variable fO_2 (FMQ+0.5, FMQ, FMQ-0.5, and FMQ-1). Samples were first heated to 1300 °C in order to melt the starting material, cooled by 10 °C per hour to the desired temperature, and held at the temperature and fO_2 of interest for 7 days. These experiments were carried out to supplement previous work (Stolper and McSween 1979; McCoy and Lofgren 1999) at these relatively low temperatures where magnetite may or may not be stable.

In addition to our three new series, we have used run products from several previous studies to help constrain the redox systematics of shergottitic liquids. First, several experiments from the study of McCoy and Lofgren (1999) were analyzed: two glasses produced at FMQ and FMQ+2, and one magnetite-glass pair equilibrated at FMQ+4. Second, a series of glasses from the study of Righter et al. (2009) was used to constrain the effect of temperature, at fixed pressure of 0.8 GPa. These latter glasses are of shergottite bulk composition equilibrated with sulfide liquids between 1200 and 1500 ºC, and contain between 2500 and 3500 ppm S (Righter et al. 2009).

3.0 Analytical methods

Glasses and crystals from shergottite experiments, and oxides from the redox sensor experiments were analyzed by electron microprobe for major and minor elements using standard approaches (e.g., Righter et al. 2009). Results for the glass and mineral phase analyses are presented in Tables 3 and 4.

Mössbauer (MB) spectra were obtained at room temperature and in backscatter measurement geometry on the same thick sections used for electron microprobe analyses using spectrometers (ESPI, Inc) similar to the ones onboard the Mars Exploration Rovers (Klingelhoefer et al. 2003). This measurement geometry does not require sample preparation (e.g., removing the glass from the thick sections and grinding them to a fine powder) and preserves the thick sections for study at a later time. The computer programs MERView and MERFit were used, respectively, to velocity calibrate and least-squares fit the spectra (Agresti et al. 2006; Agresti and Gerkines 2009). The glass MB spectra were fit with two Fe^{2+} doublets and one Fe^{3+} doublet all with Lorentzian lineshapes (Table 5). During the fitting procedures, the areas of peaks in each doublet were constrained equal, the peak widths of the Fe^{3+} doublet were constrained equal, and the peak widths of the two Fe^{2+} doublets were constrained to be the same. For glasses having low Fe^{3+} subspectral areas (all samples except Sherg1, FMQ+3) , values for the peak positions and widths were constrained to the values obtained from that sample. This model for the fitting procedure always converged and did not give physically impossible results (e.g., negative subspectral areas and linewidths <0.20 mm/s). The result that the backscatter spectra were fit with Lorentzian lineshapes implies that thickness effects, which can be important in transmission measurements if >10 mg/cm^2 of Fe is present in the sample (e.g., Greenwood and Gibb, 1971), are unlikely. The values of the center shift (δ) are reported with respect to metallic iron foil at

163 room temperature. The uncertainties on the MB parameters (Table 5) are based on various
164 independent fits described in more detail by Morris et al. (2006a).

165 The subspectral areas include a correction factor (the *f*-factor) to account for differences
166 in the recoil-free fractions of Fe^{2+} and Fe^{3+} ($f(Fe^{3+})/f(Fe^{2+})$ = 1.21 independent of mineralogical
167 composition). The value of 1.21 is the average value of *f*-factors compiled by De Grave and Van
168 Alboom (1991) for a variety of Fe-bearing silicate and oxide phases. Morris et al. (1995), using
169 this value, report good agreement between $Fe^{3+}/\Sigma Fe$ determined independently by Mössbauer
170 and by wet chemistry (WC) for a series of impact melt rocks $((Fe^{3+}/\Sigma Fe)_{MB}/(Fe^{3+}/\Sigma Fe)_{WC}$ = 1.05
171 ± 0.06 for the mean value and average deviation from the mean). More recently, Wilke et al.
172 (2005) reported values of $Fe^{3+}/\Sigma Fe$ for basaltic glasses from WC and MB measurements, but
173 without using a *f*-factor correction for the MB data. From their data (7159V starting material),
174 we calculate $(Fe^{3+}/\Sigma Fe)_{MB}/(Fe^{3+}/\Sigma Fe)_{WC}$ = 1.15 ± 0.11 as the mean value and average deviation
175 from the mean without the *f*-factor correction. When we recalculate using the *f*-factor correction,
176 the value for the ratio is 1.02 ± 0.06, bringing the two methods into significantly better
177 agreement. In summary, the value of $Fe^{3+}/\Sigma Fe$ calculated from Mössbauer spectra systematically
178 overestimates the Fe^{3+} unless the *f*-factor correction is made, as pointed out previously by
179 Ottonello et al. (2001).

180 Measurements of Fe^{3+} and Fe^{2+} from high pressure glasses and samples that are a mixture of
181 crystal and glass (series B and C) were also made using Fe K edge micro-XANES spectra (X-ray
182 absorption near edge structure) obtained at the GSECARS 13-ID-C beamline at the Advanced
183 Photon Source (Argonne National Lab). XANES has the advantage of good spatial resolution –
184 an important capability when analyzing smaller area high pressure glasses, and also samples with
185 mineral – melt mixtures. A monochromatic X-ray beam from a Si(111) double crystal

monochromator was focused onto the sample and the Fe Kα fluorescent X-ray yield was plotted as a function of incident X-ray energy (more detail on theory can be found in Bajt et al. 1994). The first derivative peak of Fe metal foil (7112 eV) was used to calibrate energy for the system. Spectra were collected between 7012 to 7493 in several regions with a 2 s dwell at each energy step: 5 eV steps from 7012 to 7102, 0.2 eV steps across the pre-edge peak from 7102 to 7137, and 2.0 eV steps from 7137 to 7163, and finally 3 eV steps from 7163 to 7493. Typically 3 to 4 scans were collected per sample, with each 10 minute scan averaged or merged in Athena (Ifeffit package; Newville 2001). Spectra were fit using the PAN routine written by R. Dimeo (2002) for IDL. A damped harmonic oscillator (DHO) was used for the background (see e.g., Cottrell et al. 2009), and Lorentzian functions were used for the Fe^{2+} and Fe^{3+} peaks. Energy fit range was limited to 7108 - 7119 eV and the FWHM of Lorentzians was fixed at 2.3 eV. Fe-bearing glasses analyzed independently using Mössbauer spectroscopy (FMQ+3 to FMQ-3; Table 2) were used to calibrate valence vs. centroid energy (area-weighted average energy of the pre-edge multiplets) using a second order polynomial (**Figure 5**), and results are presented in Table 6. The 2σ uncertainty on the XANES measurements corresponds to ±0.025 $Fe^{3+}/\Sigma Fe$ which is a combination of the MB spectroscopy error and the uncertainty from the 2nd order polynomial fit.

4.0 Results

4.1.1 Redox state of iron for a shergottite at FMQ-3 to FMQ+3.

The series of glasses produced at 1 bar and variable fO_2 cover the range over which iron-bearing glasses are converted from nearly all Fe^{2+} to nearly all Fe^{3+}, and also cover the range of fO_2 recorded in martian meteorites. Over this range, $Fe^{3+}/\Sigma Fe$ starts at as low as 0.01 at FMQ-3 and becomes as high as 0.28 at FMQ+3 (**Fig. 6**). The smooth curve from FMQ-3 to FMQ+3 is

in contrast to the various individual measurements that fall above and below these values from several previous studies. Our new data suggest a more systematic variation with fO_2, as one might expect and as has been observed for other terrestrial melt compositions, as discussed below.

4.1.2 Redox state of iron in shergottite melt with variable P_2O_5

From work on terrestrial systems, Fe^{3+}-P^{5+} complexing is known to affect the overall $Fe^{3+}/\Sigma Fe$ ratios independently of fO_2 (Horng et al. 1999). Therefore, a series of experiments with variable P_2O_5 contents, but constant temperature and fO_2 (FMQ and 1250 ºC) was carried out. For this shergottite composition, the effect of P_2O_5 is small, but nonetheless systematic, causing a change in $Fe^{3+}/\Sigma Fe$ of 0.03 across 3 wt% P_2O_5 (**Figure 7**). However, it is important to note that the magnitude of this variation (0.03 $Fe^{3+}/\Sigma Fe$) is very close to the uncertainty associated with the measurements (0.02 $Fe^{3+}/\Sigma Fe$), so this is a relatively small effect. Because shergottites can have as much a 3 wt% P_2O_5, (e.g., Kring et al. 2003; Dreibus et al. 1982) this may nonetheless be important to define when calculating $Fe^{3+}/\Sigma Fe$ for martian melts.

4.2: Effect of temperature and pressure

The effect of temperature can be constrained using the series of samples from Righter et al. (2009) covering the temperature range from 1200 to 1500 ºC. There is no detectable change in $Fe^{3+}/\Sigma Fe$ across this temperature range, with values ranging from 0.02 to 0.03. The effect of pressure can be constrained from our series of experiments between 0.8 and 4 GPa. Over this pressure range, $Fe^{3+}/\Sigma Fe$ decreases from 0.080 (±0.025) to 0.025 (±0.025). Therefore, pressure has a small negative effect on $Fe^{3+}/\Sigma Fe$, which will also be important to quantify for a full

understanding of $Fe^{3+}/\Sigma Fe$ in martian magmas, because they may be generated at pressures as high as 4 to 5 GPa.

4.3: Phase equilibrium results – magnetite stability

For a Zagami bulk composition, McCoy and Lofgren (1999) reported magnetite at FMQ+4 and 1150 ºC, but no magnetite at FMQ+2 and 1150 ºC (**Figure 8 A,B**). We measured the $Fe^{3+}/\Sigma Fe$ in both of their glasses using micro-XANES, and found the FMQ+4 glass to be 0.80, compared to 0.15 in the FMQ+2 glass. In this fO_2 range, the amount of Fe^{3+} increases substantially, making magnetite stable at > FMQ+2. In the subliquidus series C experiments in this study, magnetite is stable at 1000 ºC and FMQ-1, but not present at 1050 ºC nor any fO_2 investigated between FMQ+1 and FMQ-1 (**Figure 8 C,D)**. At temperatures above 1000 ºC, no magnetite or ilmenite is observed using optical and/or back scattered electron imaging. The glass co-existing with magnetite has a $Fe^{3+}/\Sigma Fe$ of 0.03(±0.025). Finally, for bulk composition "sherg6", magnetite and ilmenite are stable at 1050 ºC and both FMQ-0.5 and FMQ-1 (**Fig. 8 E,F**). However, $Fe^{3+}/\Sigma Fe$ of co-existing glass was not measured because the glassy areas are too small to analyze using even micro-XANES without overlap with neighboring phases. However, the results from this more MgO-rich bulk composition will be used (section 5.6) together with the new results from Zagami-like compositions from this study and that of McCoy and Lofgren (1999) to help constrain the stability field of magnetite in martian basaltic compositions.

5.0 Discussion

5.1 fO_2 dependence of $Fe^{3+}/\Sigma Fe$ and comparison to terrestrial systems

Comparison of our results to those of previous workers shows that there is some overlap with values predicted by the expression of Kress and Carmichael (1991), but the expression of

Jayasuriya et al. (2004) predicts values that are too high by a factor of 2 (**Figure 3**). This may result because Jayasuriya et al. (2004) used synthetic diopside-anorthite eutectic melt composition glasses with 1% FeO (total).

However, in the low fO_2 range, our new measurements of $Fe^{3+}/\Sigma Fe$ at FMQ-3 to FMQ are lower than calculated values using the expression of Kress and Carmichael (1991) (**Figure 3**). This is a critical fO_2 range for martian magmas because many shergottites fall within FMQ-3 to FMQ (Righter et al. 2008; Herd 2008). The lower values for the FeO-rich shergottites are evident when compared to particular terrestrial compositions like Juan de Fuca Plate basalt and Kilauea basalt (**Fig. 6**). The Kress and Carmichael (1991) and Jayasuriya et al. (2004) expressions should not be used to calculate $Fe^{3+}/\Sigma Fe$ ratios for martian magmas because they over-estimate by 100% the $Fe^{3+}/\Sigma Fe$ for shergottites in the range of fO_2 relevant to the natural setting.

Our new results resolve discrepancies with previous work. The results of Morris et al. (2008a) for basaltic glass having Mars-like compositions are consistent with our new results, with the exception of one glass sample at FMQ+2.5. This sample has a $Fe^{3+}/\Sigma Fe$ ratio that is much lower than these new results, as well as the previous work of McCanta et al. (2004). This glass has a high FeO content like all the others, and there is no compositional difference that might explain the divergent results. This data point is considered anomalous because it is in disagreement with several studies. Similarly, the datapoint of McCanta et al. (2004) at FMQ is at a $Fe^{3+}/\Sigma Fe$ value of nearly 0. At this fO_2, there should be a small percentage of ferric iron, as found in our systematic series (0.07), by Morris et al. (2008a) (0.03) and as measured by using a sample equilibrated at FMQ by McCoy and Lofgren (1999) (0.02). This nearly Fe_2O_3 – free

result of McCanta et al. (2004) is also considered anomalous because it is in disagreement with the findings of the three other studies.

5.2: Phosphorus

The role of phosphorus (P) in FeO-bearing silicate melts is important to define (Horng et al. 1999). Phosphorus is well known to stabilize Fe^{2+} (Horng et al. 1999; Mysen and Richet 2005), and this is suspected in the case of martian magmas for several reasons. First, martian magmas in general contain a significant amount of P_2O_5 – up to 5 modal % apatite (Mikouchi et al. 1998; Kring et al. 2003). Second, in terrestrial ferrobasalts, P_2O_5 has been shown to suppress magnetite stability (Toplis et al. 1994).

Our results for up to 3 wt% P_2O_5 show that there may be a small decrease in $Fe^{3+}/\Sigma Fe$ from 0.07 (±0.02) to 0.05 (±0.02) but the decrease is not significant within analytical error (Fig. 7). Even if the decrease is real, the magnitude of the range is small relative to the effects of fO_2 and pressure. Instead, the effect of P_2O_5 on magnetite stability may be due to formation of Fe^{3+}-(PO_4) melt complexes. Magnetite de-stabilization may be due to complexing of Fe^{3+} and P^{5+} in silicate melt, rather than any increase or decrease in $Fe^{3+}/\Sigma Fe$ due to addition of P_2O_5:

$$Fe_3O_4 \text{ (mgnt)} + P_2O_5 \text{ (melt)} = 2Fe^{3+}\text{-} (P^{5+}O_4)^{3-} \text{ (melt)} + FeO \text{ (melt)} \quad (1)$$

Such melt complexing would explain the de-stabilization of magnetite in P_2O_5 rich melts, and at the same time be consistent with a slight to no chemical effect of P_2O_5 addition to melt $Fe^{3+}/\Sigma Fe$ observed in our series of measurements on P_2O_5 variable glasses.

5.3: Temperature

The effect of temperature observed in our series is similar to that calculated by Kress and Carmichael (1991), as indicated in **Figure 9a** where calculations are carried out for basalt at 1 GPa and at the FMQ buffer. This lack of temperature dependence (or very weak dependence that may be within the analytical uncertainty) is also seen in the dataset of Jayasuriya et al. (2004) (**Figure 3**) where curves calculated at 1000 and 1300 ºC are nearly identical. Our study is in agreement with these previous results and shows that temperature has only a small effect on the $Fe^{3+}/\Sigma Fe$ in FeO-rich melts.

5.4: Pressure

The effect of pressure is larger, and potentially more important than temperature. Our results at elevated pressures are similar to predictions and measurements in three previous studies. Kress and Carmichael (1991) calculated a small decrease in $Fe^{3+}/\Sigma Fe$ in terrestrial basalt compositions. O'Neill et al. (2006) and Mysen and Virgo (1985) both calculated and measured a decrease in $Fe^{3+}/\Sigma Fe$, albeit at higher fO_2. However, the O'Neill et al. (2006) results are for a very high $Fe^{3+}/\Sigma Fe$ (0.7 to 0.8) and therefore not relevant to many natural systems. The effect of pressure measured in our study is compared to the findings of Kress and Carmichael (1991) in **Fig 9b**, where $Fe^{3+}/\Sigma Fe$ at 1400 ºC between 1 bar and 4.0 GPa is calculated for comparison (see also **Fig. 3**).

Determinations of the partial molar volumes and compressibilities of Fe^{3+} and Fe^{2+} in silicate melts at low pressures (e.g., Kress and Carmichael 1991; Lange and Carmichael 1987), as well as the higher pressure (0.4 to 4 GPa) results of our study (and Mysen and Virgo 1985; O'Neill et al. 2006), indicate that: a) compression at constant $Fe^{3+}/\Sigma Fe$ causes silicate melts to become more reduced (relative to FMQ), or conversely b) Fe^{3+} stability in melts is increased at higher pressure but fixed relative fO_2. This is because the low pressure partial molar volume of

316 FeO in silicate melts is much smaller than that of Fe_2O_3 in this pressure range (Kress and
317 Carmichael 1991).

318 *5.5: New model for prediction of $Fe^{3+}/\Sigma Fe$ in FeO-rich liquids.*

319 The mismatch between measured and calculated $Fe^{3+}/\Sigma Fe$ for shergottites using either the
320 Kress and Carmichael (1991) or the Jayasuriya et al. (2004) predictive expression illustrates the
321 need for developing an expression that is appropriate for high FeO martian basalt compositions.
322 Our goal here is to develop a customized expression that is applicable to high FeO melts (15 to
323 22 wt% FeO (total)).

324 Our new glasses cover a systematic range of FMQ+3 to FMQ-3, 1250 to 1600 ºC, and
325 0.0001 to 4 GPa, and we use these data to calculate a predictive expression for Fe^{3+}/Fe^{2+} in FeO-
326 rich magmas. Because there is some variability in FeO, P_2O_5, and alkalis, melt compositional
327 effects must also be accommodated in the expression. Following the procedure outlined by
328 Kress and Carmichael (1991) we derive the following expression:

329 $$\ln(Fe^{3+}/Fe^{2+}) = \mathbf{a}\ln fO_2 + \mathbf{b}/T + \mathbf{c}P/T + \mathbf{d}X_{FeO} + \mathbf{e}X_{Al2O3} + \mathbf{f}X_{CaO} + \mathbf{g}X_{Na2O} + \mathbf{h}X_{K2O} + \mathbf{i}X_{P2O5} + \mathbf{j} \quad (2)$$

330 Fitting the above equation to our 22 experiments results in a series of regression coefficients that
331 can be used to predict Fe^{3+}/Fe^{2+} for martian melts (Table 7).

332 To illustrate the utility of such an expression in application to martian magma genesis, we
333 use two examples for martian meteorites – basaltic shergottite and a nakhlite parent melt which
334 is similar to shergottites in composition but more oxidized (FMQ vs. FMQ-2 or FMQ-3. We
335 have calculated PT curves for a shergottitic melt composition that has a constant $Fe^{3+}/\Sigma Fe$ ratio
336 of 0.02, 0.03, 0.05 and 0.08 (**Fig. 10**). As can be seen, a melt starting at a pressure of 4 GPa and
337 rising to the surface will become more oxidized by approximately one log fO_2 unit. This

suggests that the nakhlite parent magmas, which equilibrated at shallow pressures near FMQ (Righter et al. 2008), may have originated at a lower fO_2 in the deep martian mantle – perhaps FMQ-1. Also, it suggests that a melt formed at a shallower depth in the martian mantle, such as primary shergottite liquid (1 to 1.5 GPa; Filiberto et al. 2008; Musselwhite et al. 2006) will not become significantly oxidized as it ascends to the surface.

5.6: Magnetite Stability

Many previous experiments define magnetite stability in terrestrial melt compositions (**Fig. 1**). Magnetite becomes stable at higher FeO content of silicate melts as $Fe^{3+}/\Sigma Fe$ decreases. This suggests that martian silicate melts with FeO (total) contents of ~ 20 wt% may be able to saturate or stabilize magnetite at $Fe^{3+}/\Sigma Fe$ values as low as 0.05. We can evaluate this possibility with experiments from series C. All experiments with stabilized magnetite have very low $Fe^{3+}/\Sigma Fe$ ratios, <0.05. Toplis and Carroll (1995) showed that the temperature of magnetite stability in a ferrobasalt composition (13.4 to 14.6 wt% FeO (total)) is a strong function of fO_2 (**Fig. 11a**). Comparison of our new results at FMQ-1, FMQ+2, and FMQ+4 show that high FeO (total) (15 to 22 wt%) shergottite liquids stabilize magnetite about 50 °C lower than is observed for terrestrial magmas with lower FeO contents (**Fig. 11a**).

Toplis and Carroll (1995) also showed that magnetite stability is dependent on temperature and melt Fe_2O_3 content (**Fig. 11b**). Magnetite becomes stable at any given temperature at a certain threshold Fe_2O_3 content. Toplis and Carroll (1995) utilize the expression of Kress and Carmichael (1991) to calculate Fe_2O_3 in the ferrobasaltic melts, as the latter expression was calibrated in this compositional range. However, to compare our results to those of the terrestrial compositions, we will use our expression for Fe_2O_3 that is based on the high FeO shergottite melts. The calculated Fe_2O_3 contents for our 1000 °C experiments and also for the 1150 °C

experiment (ZAG 064) from McCoy and Lofgren (1999) are shown in **Fig. 11b** and illustrate that the linear relation proposed by Toplis and Carroll (1995) holds at these high and low Fe_2O_3 ends of the series.

In summary, magnetite saturation in shergottite liquids occurs at lower temperatures compared to terrestrial liquids because the $Fe^{3+}/\Sigma Fe$ ratio of shergottite liquids remains lower than terrestrial basaltic liquids in the range between FMQ-3 to FMQ+1. Both of these factors lead to the conclusion that it is more difficult to stabilize magnetite in martian melts than in terrestrial melts.

5.8: Implications

If the commonly observed surficial magnetite on Mars (e.g., at MER sites) is igneous in origin, it must originate in one of two ways. First, it is not a near liquidus phase at any fO_2 between FMQ+1 to FMQ-3, but it becomes a liquidus phase at higher fO_2, or possibly in more evolved or fractionated liquids, neither of which is represented in the martian meteorite collection. That is, martian magmas with near-liquidus magnetite may have equilibrated at higher fO_2 than is typically recorded in martian meteorites (>FMQ buffer). This may not be surprising, because differences in ages, bulk compositions, and mineral phases between martian meteorites and findings of robotic missions have been noted before (e.g., Hamilton and Minitti 2003; McSween et al. 2009).

A second possibility is that the magnetite formed during cooling below 1000 °C, at typical fO_2 for martian meteorites – FMQ to FMQ-1. This is consistent with the presence of Ti-bearing magnetite and/or by the occurrence of magnetite as skeletal crystals in mesostasis or inclusions in silicate mineral grains. In the literature, magnetite in martian meteorites is

ubiquitously reported as Ti-bearing magnetite and/or magnetite with skeletal and euhedral texture (e.g., Stolper and McSween 1979; Vieira et al. 1986; McSween 1994; Dyar et al. 2005; Treiman 2005; Morris et al. 2008b). However, the modal abundance is only a few percent, which is lower than the amount observed at Gusev Crater (~ 10%).

A third possibility is that the magnetite is secondary in origin. We cannot exclude this possibility, but an igneous origin is evidenced by magnetic material sampled by the Mars Exploration Rover Spirit at the Gusev landing site that is chemically enriched in Fe and Ti, implying the presence of titanomagnetite (Morris et al. 2008a). In fact, Adirondack Class basalts at Gusev crater and martian meteorite MIL 03346 have comparable magnetite contents on the basis of Mössbauer measurements (Morris et al. 2006a, 2006b) and FeO (total) concentrations (both have ~19 wt. % FeO (total) (Gellert et al. 2006; Day et al. 2006)). Five rocks at Gusev crater have 45 to 54% of their total iron present as magnetite for FeO + Fe_2O_3 concentrations between 17 and 21 wt.% (Morris et al. 2008a). In addition, serpentinite and other secondary origins for magnetite usually are associated with nearly pure Fe magnetite, with little to no TiO_2 (e.g., Gahlan et al. 2006). For these reasons, we favor a < 1000 °C igneous origin for the magnetite, perhaps formed upon cooling.

If the redox state of martian magmas is controlled by polybaric carbon-iron equilibria, as proposed by Righter et al. (2008), it implies origination at greater depths (pressures of 3 to 4 GPa). Such melts, upon decompression, will become more oxidized. Calculations based on the previous work of Kress and Carmichael (1991) suggested that fO_2 may be increased by approximately 1 log fO_2 unit, and our new work has confirmed this magnitude of an effect for FeO-rich martian melts. Decompression of a high FeO melt will only lead to fO_2 that is higher by one log fO_2 unit (**Figure 10)**. Therefore decompression will allow some oxidation, but not as

much as expected from a terrestrial basalt. Because dry deep magmas are likely to be too dense to ascend through the crust, deeper magmas would have to be volatile-bearing, perhaps with a few wt% H_2O, so that the densities could be lowered enough to be buoyant and ascend through the crust (**Figure 12**). Water has been suggested to be a factor in various aspects of martian magmas (e.g., Lentz et al. 2001; Dann et al. 2001; Medard and Grove 2006). Hydrous conditions might also increase the $Fe^{3+}/\Sigma Fe$ ratio and thus expand the magnetite stability field (Minitti and Rutherford 2000). Even though experimental evidence from basaltic systems suggests water is not a significant oxidant (Moore et al. 1995; Botcharnikov et al. 2005), the high FeO martian systems may have different behavior. But, the higher FeO martian melts would require a proportionately larger effect of water on the $Fe^{3+}/\Sigma Fe$ to alter the ratio significantly. Nonetheless, in future experiments, the effect of dissolved water on melt $Fe^{3+}/\Sigma Fe$ will be explored.

6.0 Summary and Conclusions:

One bar shergottite composition glasses equilibrated at FMQ-3 to FMQ+3 show a significantly lower $Fe^{3+}/\Sigma Fe$ than terrestrial basalts equilibrated at the same conditions. As melt P_2O_5 contents increase from 0 to 3 wt% (at fixed pressure, temperature and fO_2), $Fe^{3+}/\Sigma Fe$ changes from 0.07 (±0.02) to 0.05 (±0.02), within analytical error. Temperature increases between 1200 and 1500 °C similarly cause no measurable variation in $Fe^{3+}/\Sigma Fe$. Pressure increases from 1 to 4 GPa causes a decrease of 0.06 in the $Fe^{3+}/\Sigma Fe$. The trends with pressure and temperature are in agreement with results of previous studies. Combining our new series of data allows derivation of an expression to calculate Fe^{3+}/Fe^{2+} for high FeO melts such as martian magmas:

$$\ln(Fe^{3+}/Fe^{2+}) = a\ \ln fO_2 + b/T + cP/T + dX_{FeO} + eX_{Al2O3} + fX_{CaO} + gX_{Na2O} + hX_{K2O} + iX_{P2O5}.$$

This expression can be used to show that decompressed FeO-rich melts become slightly more oxidized upon ascent to the surface (compared to 4 GPa). Magnetite stability is suppressed by the lower Fe^{3+}/Fe^{2+} of the high FeO melts, and low $Fe^{3+}/\Sigma Fe$ in martian melts will have important controls on phase equilibria. Magnetite stability is a function of Fe_2O_3 and temperature and is stable ~50 °C lower than typical terrestrial basalt. Difficulty in producing magnetite in near liquidus magmatic systems indicates that many martian basalts could be more oxidized than FMQ (and not represented in meteorite collections), or that the magnetite formed upon cooling below 1000 °C, consistent with the presence of titano-magnetite in the groundmass of shergottites and the mesostasis of nakhlites. Alternatively, magnetite may have a secondary origin, but such magnetites are expected to be TiO_2-free; compositional measurements on magnetic particles indicate Ti-bearing magnetite at Gusev crater.

7.0 Acknowledgements

We would like to thank M. Toplis and T. McCoy for discussions relating to redox equilibria in martian magmas, and to T. McCoy for loaning samples from his experimental study. Loan Le provided assistance in the gas mixing furnace lab, and Anne Peslier and Kent Ross provided assistance with the electron microbeam analysis. This research was supported at NASA-JSC by an RTOP to KR from the NASA Mars Fundamental Research program. Portions of this work were performed at GeoSoilEnviroCARS (Sector 13), Advanced Photon Source (APS), Argonne National Laboratory. GeoSoilEnviroCARS is supported by the National Science Foundation - Earth Sciences (EAR-1128799) and Department of Energy - Geosciences (DE-FG02-94ER14466). Use of the Advanced Photon Source was supported by the U. S. Department of

Energy, Office of Science, Office of Basic Energy Sciences, under Contract No. DE-AC02-06CH11357.

8.0 References

Agresti, D.G., M.D. Dyar, and M.W. Schaefer (2006) Velocity scales for Mars Mössbauer data, Hyperfine Interactions, 170, 67-74.

Agresti, D.G. and Gerakines, P.A. (2009) Simultaneous Fitting of Mars Mössbauer Data. Hyperfine Interactions, 188, 113-120.

Bajt, S., Sutton, S.R., and Delaney, J.S. (1994) X-ray microprobe analysis of iron oxidation states in silicates and oxides using X-ray absorption near edge structure (XANES). Geochimica et Cosmochimica Acta, 58, 5209-5214.

Berry, A.J., Danyushevsky, L.V., O'Neill, H.St.C., Newville, M. and Sutton, S.R. (2008) Oxidation state of iron in komatiitic melt inclusions indicates hot Archaean mantle**.** Nature, 455, 960-963.

Bose, K. and Ganguly, J. (1995) Quartz-coesite transition revisited: Reversed experimental determination at 500-1200°C and retrieved thermochemical properties. American Mineralogist, 80, 321-238.

Botcharnikov, R.E., Koepke, J., Holtz, F., McCammon, C., and Wilke, M. (2005) The effect of water activity on the oxidation and structural state of Fe in a ferrobasaltic melt, Geochimica et Cosmochimica Acta, 69, 5071-5085.

Cottrell, E., Kelley, K.A., Lanzirotti, A. and Fischer, R.A. (2009) High precision determination of iron oxidation state in silicate glasses using XANES. Chemical Geology, 268, 167–179.

Dann, J.C., Holzheid, A.H., Grove, T.L. and McSween, H.Y. (2001) Phase equilibria of the Shergotty meteorite: Constraints on pre-eruptive water contents of martian magmas and fractional crystallization under hydrous conditions. Meteoritics and Planetary Science, 36, 793–806.

Day, J. M. D., L. A. Taylor, C. Floss, and H. Y. McSween Jr. (2006), Petrology and chemistry of MIL 03346 and its significance in understanding the petrogenesis of nakhlites on Mars, Meteoritics & Planetary Science, 41, 581-606.

Dreibus, G., Palme, H., Ramensee, W., Spettel, B., Weckwerth, G., and H. Wanke (1982) Composition of Shergotty Parent Body: Further Evidence for a Two Component Model of Planet Formation. Thirteenth Lunar and Planetary Science Conference, Abstract #1096.

Dyar, M.D., A.H. Treiman, C.M. Pieters, T. Hiroi, M.D. Lane, and V. O'Conner (2005), MIL03346, the most oxidized Martian meteorite: A first look at spectroscopy, petrography, and mineral chemistry. Journal of Geophysical Research: 110, E09005, doi:10.1029/2005JE002426.

Filiberto, J., Treiman, A.H., Le, L. (2008) Crystallization Experiments on a Gusev Basalt Composition. Meteoritics & Planetary Science, 43, 1137-1146.

Gahlan, H.A., Arai, S., Ahmed, A.H., Ishida, Y., Abdel-Aziz, Y.M., Rahimi, A. (2006) Origin of magnetite veins in serpentinite from the Late Proterozoic Bou-Azzer ophiolite, Anti-Atlas, Morocco: An implication for mobility of iron during serpentinization. Journal of African Earth Sciences, 46, 318–330.

Gellert, R., R. Rieder, J. Brückner, B. C. Clark, G. Dreibus, G. Klingelhöfer, G. Lugmair, D. W. Ming, H. Wänke, A. Yen, J. Zipfel, and S. W. Squyres (2006) Alpha Particle X-Ray Spectrometer (APXS): Results from Gusev crater and calibration report. Journal of Geophysical Research, 111, E02S05, 10.1029/2005JE002555.

Greenwood, N. N., and T. C. Gibb (1971) *Mössbauer Spectroscopy*, 659 pp., Chapman and Hall Ltd, London.

Hamilton, V.E. and Minitti, M.E. (2003) Are oxidized shergottite-like basalts an alternative to "andesite" on Mars? Geophysical Research Letters, 30, 1915, doi:10.1029/2003GL017839.

Herd, C. (2008) Basalts as Probes of Planetary Interior Redox State. Reviews In Mineralogy and Geochemistry, 68, 527-553.

Horng, W.-S., Hess, P.C., Gan, H. (1999) The interactions between M^{+5} cations (Nb^{+5}, Ta^{+5}, or P^{+5}) and anhydrous haplogranite melts. Geochimica et Cosmochimica Acta, 63, 2419-2428.

Jayasuriya, K.D., O'Neill, H.St.C., Berry, A.J. Campbell, S.J. (2004) A Mössbauer study of the oxidation state of Fe in silicate melts. American Mineralogist, 89, 1597-1609.

Kilinc, A. Carmichael, I.S.E., Rivers, M.L. and Sack, R.O. (1983) The ferric-ferrous ratio of natural silicate liquids equilibrated in air. Contributions to Mineralogy and Petrology, 83, 136-145.

King, P.L., Hervig, R.L., Holloway, J.R., Delaney, J.S., & Dyar, M.D. (2000) Fe^{3+}/Fe_{total} and H partitioning between amphiboles and basanitic melts as a function of oxygen fugacity. Earth and Planetary Science Letters, 178, 97-112.

513 Klingelhöfer, G., Bernhardt, B., Foh, J., et al. (2002) The Miniaturized Mössbauer Spectrometer
514 MIMOS II for Extraterrestrial and Outdoor Terrestrial Applications: A Status Report.
515 Hyperfine Interactions, 144/145, 371-379.

516 Kress, V.C. and Carmichael, I.S.E. (1988) Stoichiometry of the iron oxidation reaction in silicate
517 melts. American Mineralogist, 73, 1267-1274.

518 Kress V.C., Carmichael I.S.E. (1991) The iron redox state in silicate liquids: the effect of
519 pressure, temperature, oxygen fugacity and composition, with application to the genesis of
520 basic magma. Contributions to Mineralogy and Petrology, 108: 82–92.

521 Kring, D.A. et al. (2003) Composition of the first bulk melt sample from a volcanic region of
522 Mars: Queen Alexandra Range 94201. Meteoritics and Planetary Science, 38, 1833–1848.

523 Lange, R.A. and Carmichael, I.S.E. (1987) Densities of Na_2O-K_2O-MgO-MgO-FeO-Fe_2O_3 –
524 Al_2O_3 -TiO_2 -SiO_2 liquids: New measurements and derived partial molar properties.
525 Geochimica et Cosmochimica Acta, 51, 2931-2946.

526 Leinenweber, K., Tyburczy, J., Sharp, T., Soignard, E., Diedrich, T., Petuskey, W., Wang, Y.,
527 and Mosenfelder, J. (2012) Cell assemblies for reproducible multi-anvil experiments (the
528 COMPRES assemblies), American Mineralogist, 97, 353–368.

529 Lentz, R.F., McSween, H.Y., Jr., Ryan, J., and Riciputi, L.R. (2001) Water in martian magmas:
530 Clues from light lithophile elements in shergottite and nakhlite pyroxenes. Geochimica et
531 Cosmochimica Acta, 65, 4551–4565.

532 Lodders, K. and Fegley, B. Jr. (1997) An Oxygen Isotope Model for the Composition of Mars.
533 Icarus 126, 373–394.

McCanta, M. C. Dyar, M. D. Rutherford, M. J. Delaney, J. S. (2004) Iron partitioning between basaltic melts and clinopyroxene as a function of oxygen fugacity. American Mineralogist, 89, 1685-1693.

McCoy, T.J. and Lofgren, G.E. (1999) Crystallization of the Zagami shergottite: an experimental study. Earth and Planetary Science Letters, 173, 397-411.

McSween Jr., H. Y. (1994) What we have learned about Mars from SNC meteorites, Meteoritics, 29, 757-779.

McSween, H. Y., et al. (2006) Alkaline volcanic rocks from the Columbia Hills, Gusev crater, Mars, Journal of Geophysical Research, 111, E09S91, doi:10.1029/2006JE002698.

McSween, H.Y., Jr., Taylor, G.J. and Wyatt, M.B. (2009) Elemental composition of the Martian crust. Science, 324, 736-739.

Medard, E. and Grove, T.L. (2006) Early hydrous melting and degassing of the Martian interior. Journal of Geophysical Research, 111, E11003, doi:10.1029/2006JE002742.

Mikouchi T., Miyamoto M. and McKay G. (1998) Mineralogy of Antarctic basaltic shergottite Queen Alexandra Range 94201: Similarities to Elephant Moraine A79001 (Lithology B) martian meteorite. Meteoritics and Planetary Science, 33, 181-189.

Ming, D. W., et al. (2006), Geochemical and mineralogical indicators for aqueous processes in the Columbia Hills of Gusev crater, Mars, Journal of Geophysical Research, 111, E02S12, doi:10.1029/2005JE002560.

Minitti, M. and Rutherford, M.J. (2000) Genesis of the Mars Pathfinder “sulfur-free” rock from SNC parental liquids. Geochimica et Cosmochimica Acta, 64, 2535-2547.

555 Moore, G.M., Righter, K., and Carmichael, I.S.E. (1995) The effect of dissolved water on the
556 oxidation state of iron in natural silicate liquids. Contributions to Mineralogy and Petrology,
557 120, 170-179.

558 Morris, R.V., G. Klingelhöfer, C. Schröder, D.S. Rodionov, A. Yen, D.W. Ming, P.A. de Souza
559 Jr., I. Fleischer, T. Wdowiak, R. Gellert, B. Bernhardt, E.N. Evlanov, B. Zubkov, J. Foh, U.
560 Bonnes, E. Kankeleit, P. Gütlich, F. Renz, S. W. Squyres, and R. E. Arvidson (2006a)
561 Mössbauer mineralogy of rock, soil, and dust at Gusev Crater, Mars: Spirit's journey through
562 weakly altered olivine basalt on the Plains and pervasively altered basalt in the Columbia
563 Hills. Journal of Geophysical Research, 111, E02S13, doi:10.1029/2005JE002584.

564 Morris, R. V., G. A. McKay, D. W. Ming, G. Klingelhöfer, C. Schröder, D. Rodionov, and A.
565 Yen (2006b) Magnetite in martian meteorite MIL 03346 and Gusev Adirondack class basalt:
566 Mössbauer evidence for variability in the oxidation state of Adirondack lavas, Lunar and
567 Planetary Science, XXXVII, Abstract 1594.

568 Morris, R. V., et al. (2008a) Iron mineralogy and aqueous alteration from Husband Hill through
569 Home Plate at Gusev Crater, Mars: Results from the Mössbauer instrument on the Spirit
570 Mars Exploration Rover. Journal of Geophysical Research, 113, E12S42,
571 doi:10.1029/2008JE003201.

572 Morris, R. V., G. A. McKay, D. G. Agresti, and L. Le (2008b) Mössbauer and electron
573 microprobe studies of density separates of martian Nakhlite MIL03346: Implication for
574 interpretation of Mössbauer spectra acquired by the Mars Exploration Rovers, Lunar and
575 Planetary Science, XXXIX, Abstract 2458.

Musselwhite, D. S., H. A. Dalton, W. S. Kiefer, and A. H. Treiman (2006) Experimental petrology of the basaltic shergottite Yamato-980459: Implications for the thermal structure of the Martian mantle, Meteoritics and Planetary Science, 41, 1271-1290.

Mustard, J. F., Poulet, F., Gendrin, A., Bibring, J.-P., Langevin, Y., Gondet, B., Mangold, N., Bellucci, G., and F. Altieri (2005) Olivine and Pyroxene Diversity in the Crust of Mars. Science, 307, 1594-1597.

Mysen B. O. and Richet P. (2005) Silicate Glasses and Melts – Properties and Structure. Elsevier, New York, 548 p.

Mysen, B.O. and Virgo, D (1985) The structural state of iron in oxidized vs. reduced glasses at 1 atm: A ^{57}Fe Mössbauer study. Physics and Chemistry of Minerals, 12, 191-200.

Newville, M. (2001) IFEFFIT: interactive XAFS analysis and FEFF fitting. Journal of Synchrotron Radiation, 8, 322-324.

Nimmo, F. and Tanaka, K. (2005) Early crustal evolution of Mars. Ann. Rev. Earth Planet. Sci. 33, 133-161.

O'Neill, H.St.C. (1986) Mo-MoO_2 (MOM) oxygen buffer and the free energy of formation of MoO_2. American Mineralogist, 71, 1007-1010.

O'Neill, H.St.C. (1987) The quartz-fayalite-magnetite equilibria and free energies of formation of fayalite (Fe_2SiO_4) and magnetite (Fe_3O_4). American Mineralogist, 72: 67-75.

O'Neill, H. St. C. Berry, A. J. McCammon, C. C. Jayasuriya, K. D. Campbell, S. J. Foran, G. (2006) An experimental determination of the effect of pressure on the $Fe^{3+}/\Sigma Fe$ ratio of an anhydrous silicate melt to 3.0 GPa. American Mineralogist, 91, 404-412.

Ottonello, G., R. Moretti, L. Marini, and M. V. Zuccolini (2001), Oxidation state of iron in silicate glasses and melts: a thermochemical model. Chemical Geology, 174, 157-179.

Righter K., Yang H., Costin G., Downs R.T. (2008a) Oxygen fugacity in the Martian mantle controlled by carbon: New constraints from the nakhlite MIL 03346. Meteoritics & Planetary Science, 43, 1709-1723.

Righter, K., Humayun, M., and Danielson, L.R. (2008b) High pressure and temperature partitioning of palladium during core formation. Nature Geoscience, 1, 321-323.

Righter, K., Pando, K., Danielson, L.R. (2009) Experimental evidence for sulfur-rich martian magmas: implications for volcanism and surficial sulfur sources. Earth and Planetary Science Letters, 288, 235-243.

Ross, N. L., Akaogi, M., Navrotsky, A., Susaki, J., McMillan, P. (1986) Phase transitions among the $CaGeO_3$ polymorphs (wollastonite, garnet, and perovskite structures): Studies by high-pressure synthesis, high-temperature calorimetry, and vibrational spectroscopy and calculation. Journal of Geophysical Research, 91, 4685-4696.

Sack, R.O., I. S. E. Carmichael, M. Rivers and M. S. Ghiorso (1980) Ferric-ferrous equilibria in natural silicate liquids at 1 bar. Contributions to Mineralogy and Petrology, 75, 369−376.

Shirai, N. and Ebihara, M. (2004) Chemical characteristics of a Martian meteorite, Yamato 980459. Antarctic Meteorite Research, 17, 55-67.

Snyder, D., Carmichael, I.S.E., and Wiebe, R.A. (1993) Experimental study of liquid evolution in an Fe-rich, layered mafic intrusion: constraints of Fe-Ti oxide precipitation on the T-f_{O_2} and T-ϱ paths of tholeiitic magmas. Contributions to Mineralogy and Petrology, 113, 73-86.

Stolper, E. and McSween, H.Y. (1979) Petrology and origin of the shergottite meteorites. Geochimica et Cosmochimica Acta, 43, 1475-1498.

Taylor, J.R., Wall, V.J., and Pownceby, M.I. (1992) The calibration and application of caccurate redox sensors. American Mineralogist, 77, 284-295.

Thy, P. and Lofgren, G.E. (1994) Experimental constraints on the low-pressure evolution of transitional and mildly alkalic basalts: the effect of Fe-Ti oxide minerals and the origin of basaltic andesites. Contributions to Mineralogy and Petrology, 116, 340-351.

Toplis, M.J. and M.R. Carroll (1995) An Experimental Study of the Influence of Oxygen Fugacity on Fe-Ti Oxide Stability, Phase Relations, and Mineral—Melt Equilibria in Ferro-Basaltic Systems. Journal of Petrology, 36, 1137-1170.

Toplis, M.J. and M.R. Carroll (1996) Differentiation of Ferro-Basaltic Magmas under Conditions Open and Closed to Oxygen: Implications for the Skaergaard Intrusion and Other Natural Systems. Journal of Petrology, 37, 837-858.

Toplis, M.J., Libourel, G., and Carroll, M.R (1994) The role of phosphorus in crystallisation processes of basalt: An experimental study. Geochimica et Cosmochimica Acta, 58, 797-810.

Treiman, A.H. (2005) The nakhlite meteorites: Augite-rich igneous rocks from Mars. Chemie der Erde – Geochemistry 65, 203-270. Xirouchakis, D., Draper, D.S., Schwandt, C.S., Lanzirotti, A. (2002) Crystallization conditions of Los Angeles, a basaltic Martian meteorite. Geochimica et Cosmochimica Acta, 66, 1867-1880.

637 Vieira, V. W. A., T. V. V. Costa, H. G. Jensen, J. M. Knudsen, and M. Olsen (1986), Oxidation
638 state of iron in SNC meteorites as studied by Mössbauer spectroscopy, Physica Scripta, 33,
639 180-186.
640 Wilke, M., G. M. Partzsch, B. Bernhardt, and D. Lattard (2005) Determination of the iron
641 oxidation state in basaltic glasses using XANES at the K-edge. Chemical Geology, 220, 143-
642 161.
643 Yagi, T., Akaogi, M., Shimomura, O., Suzuki, T., Akimoto, S. (1987) In situ observation of the
644 olivine-spinel phase transformation in Fe2SiO4 using synchrotron radiation. Journal of
645 Geophysical Research, 92, B7, 6207-6214.

646

Figure Captions

Figure 1: Experiments defining the stability of magnetite in terrestrial basaltic systems (Nielsen et al. 1994; Snyder et al. 1993; Thy and Lofgren 1994; Toplis and Carroll 1995) and $Fe^{3+}/\Sigma Fe$ calculated using Kress and Carmichael (1991).

Figure 2: FeO vs. Al_2O_3 for experimental data used to predict the Fe^{3+}/Fe^{2+} in terrestrial basalt. Experimental data (from Kress 1988, Kilinc et al. 1983; Kress and Carmichael 1991; Sack et al. 1980; shergottites data from Lodders and Fegley 1999 compilation) do not overlap with the FeO* or Al_2O_3 of shergottite compositions. Shergottites are plotted as FeO* because they have not typically been analyzed for Fe_2O_3 since most (~95%) of the iron is likely FeO..

Figure 3: $Fe^{3+}/\Sigma Fe$ calculated for a Zagami-like shergottite using the expressions of Kress and Carmichael (1991) and Jayasuriya et al. (2004) along with data for FeO-rich glasses from Morris et al. (2008) and McCanta et al. (2004). Note curves are calculated whereas the plotted data points are measured.

Figure 4: Linear fit pressure calibration to solid state phase transitions for the G2 assembly. Pressure calibration was achieved using the quartz-coesite transition at 1000 °C (Bose and Ganguly 1995), the fayalite-gamma spinel transition at 1200 °C (Yagi et al. 1987), and the tetragonal garnet-orthorhombic perovskite transition of $CaGeO_3$ at 1000 °C (Ross et al. 1986). See text for more details about the assemblies.

Figure 5: Centroid peak energy vs. $Fe^{3+}/\Sigma Fe$ for a suite of high FeO silicate glass standards measured independently using Mössbauer spectroscopy. Samples used were glasses "IW", "FMQ" and "CO_2" from Morris et al. (2008a) and samples FMQ+1, FMQ+2, and FMQ+3 from this study. Data were fit with a second order polynomial: $Fe^{3+}/\Sigma Fe = 227764.5361(eV)^2 - 3239724.4555(eV) + 11520468.0971$. Centroid energy is the area-weighted average energy of the pre-edge peaks.

672 **Figure 6**: New results for glasses measured using Mössbauer spectroscopy illustrating that the
673 $Fe^{3+}/\Sigma Fe$ in shergottite composition remains low relative to curves calculated for terrestrial
674 basalts such as mid ocean ridge (JDFD2) and Hawaiian (Kil-2) basalts (from Kress and
675 Carmichael 1991). One high FeO glass from Morris et al. (2008) may be anomalously low
676 (FMQ+2.4).

677 **Figure 7**: Effect of P_2O_5 (wt%) on $Fe^{3+}/\Sigma Fe$ measured using Mössbauer spectroscopy – all
678 experiments at 1250 °C and FMQ buffer. The small variation of $Fe^{3+}/\Sigma Fe$ with P_2O_5 is within
679 analytical error, and even if it is real, it is not likely to cause magnetite destabilization.

680 **Figure 8**: Back scattered electron images of magnetite stability experiments. Magnetite is the
681 brightest phase in these images – white. A: experiment ZAG 063 (FMQ+2, 1150 °C) from
682 McCoy and Lofgren (1999) showing glass and pyroxene, but no magnetite; B: experiment ZAG
683 064 (FMQ+4, 1150 °C) from McCoy and Lofgren (1999) showing glass, pyroxene, and
684 magnetite (bright phase); C: experiment FMQ-1, 1050 °C, in which there is glass and pyroxene,
685 but no magnetite; D: experiment FMQ-1, 1000 °C in which there is glass, pyroxene, and
686 magnetite; E: FMQ-1, 1050 °C for sherg 6 composition shows glass, pyroxene, feldspar,
687 magnetite and phosphate; F: FMQ-0.5, 1050 °C for sherg 6 composition shows glass, pyroxene,
688 feldspar, magnetite, ilmenite, and phosphate.

689 **Figure 9a**: Effect of temperature on $Fe^{3+}/\Sigma Fe$ for shergottite glasses at 1 GPa, FMQ-2 and
690 variable temperature (shown as solid circles). This suite of glasses is from Righter et al. (2009)
691 and contain between 1800 and 2800 ppm S. Shown for comparison are calculations using the
692 expression of Kress and Carmichael (1991) for 1 GPa at FMQ. **Figure 9b**: Effect of pressure on
693 $Fe^{3+}/\Sigma Fe$ for shergottite glasses at 1500 ºC and variable pressure (solid circles). Shown for
694 comparison are calculations using the expression of Kress and Carmichael (1991) for 1400 ºC
695 and FMQ-1. 1400 ºC was used for comparison because if 1500 ºC was used the data overlap
696 entirely with our data making the plot difficult to read.

697 **Figure 10**: Calculation of ΔFMQ vs. pressure (with adiabatic gradient of 0.18K/km), for four
698 different values of $Fe^{3+}/\Sigma Fe$: 0.02, 0.03, 0.05 and 0.08. All indicate that a melt that is
699 decompressed will become more oxidized by the time it reaches the surface, by approximately 1
700 log fO_2 unit. Curves calculated using equation (2) and the constants derived from multiple linear
701 regression in Table 7.

Figure 11a: Comparison of magnetite saturation conditions (T and fO_2) for a terrestrial ferrobasalt (Toplis and Carroll 1995) and a martian shergottite (this study). High FeO shergottite melts saturate magnetite about 50 °C lower than terrestrial basalt. Solid line is upper limit for magnetite in terrestrial compositions, and dashed line is the upper limit for magnetite in high FeO shergottitic compositions. **Figure 11b**: $\ln(Fe_2O_3)$ vs. 10000/T for terrestrial basalt studies (Snyder et al. 1993; Thy and Lofgren 1994; Toplis and Carroll 1994, 1995) and our results for high FeO shergottite melts. The general trend defined by terrestrial studies holds true for martian melt compositions as well at higher and lower temperatures than the terrestrial work. Solid line defines the boundary between magnetite-bearing and magnetite-free experiments.

Figure 12: Deeper magmas will be denser, but that may be offset by having volatiles (e.g., H_2O or CO_2) dissolved in the magma that will lower the density by as much as 0.2 g/cm^3. Plotted are densities and Mg# for liquids derived from fractional crystallization of Yamato 980459 composition (Shirai and Ebihara 2004) at 1 bar, 1.0 GPa (both no water), and with 3 wt% water at 1.0 GPa. All calculations done with MELTS algorithm (Ghiorso and Sack 1995) with fixed relative fO_2 of FMQ buffer. Mars crustal density from Nimmo and Tanaka (2005). Densities were taken from MELTS results, which are calculated using Lange and Carmichael (1987).

719 **Table 1: Starting compositions**

Oxides	Sherg 6	Sherg 1
SiO_2	50.0	53.00
TiO_2	1.3	1.30
Al_2O_3	10.0	5.00
FeO	18.5	21.00
MnO	0.30	0.30
MgO	8.5	5.00
CaO	8.50	10.50
Na_2O	1.6	1.60
K_2O	0.3	0.30
P_2O_5	0.6	0.60
Total	99.60	98.60

720

721

722

723 **Table 2: Experimental run conditions**

Run #	Δ FMQ[d]	Duration	Pressure	Temp. (ºC)	composition	Run products	Capsule or loop
Sh1-FMQ+3	+3	72 hrs	1 bar	1250	Sherg 1	glass	Re loop
Sh1-FMQ+2	+2	72 hrs	1 bar	1250	Sherg 1	glass	Re loop
Sh1-FMQ+1	+1	72 hrs	1 bar	1250	Sherg 1	glass	Re loop
Sh1-FMQ	0	72 hrs	1 bar	1250	Sherg 1	glass	Re loop
Sh1a-FMQ	0	72 hrs	1 bar	1250	Sherg 1	glass	Re loop
Sh1b-FMQ	0	72 hrs	1 bar	1250	Sherg 1	glass	Re loop
Sh1c-FMQ	0	72 hrs	1 bar	1250	Sherg 1	glass	Re loop
Sh1-FMQ-1	-1	72 hrs	1 bar	1250	Sherg 1	glass	Re loop
Sh1-FMQ-2	-2	72 hrs	1 bar	1250	Sherg 1	glass	Re loop
Sh1-FMQ-3	-3	72 hrs	1 bar	1250	Sherg 1	glass	Re loop
ZAG-053 [a]	0	72 hrs	1 bar	1260	Synth. Zagami	Glass	Pt loop
ZAG-063 [a]	+2	72 hrs	1 bar	1150	Synth. Zagami	Glass	Pt loop
ZAG-064 [a]	+4	72 hrs	1 bar	1150	Synth. Zagami	Glass + magt	Pt loop
IW [c]	-3.5	16 hrs	1 bar	1300	Mars global avg. soil	Glass	Pt cruc.
FMQ [c]	0	16 hrs	1 bar	1300	Mars global avg. soil	Glass	Pt cruc.
CO2 [c]	+7	16 hrs	1 bar	1300	Mars global avg. soil	Glass	Pt cruc.
Sh1-1050-FMQ-1	-1	96 hrs	1 bar	1050	Sherg 1	Glass, pyrox	Re loop
Sh1-1050-FMQ-0.5	-0.5	96 hrs	1 bar	1050	Sherg 1	Glass, pyrox	Re loop
Sh1-1050-FMQ	0	96 hrs	1 bar	1050	Sherg 1	Glass, pyrox	Re loop
Sh1-1050-FMQ+0.5	+0.5	96 hrs	1 bar	1050	Sherg 1	Glass, pyrox	Re loop
Sh6-1050-FMQ-1	-1	96 hrs	1 bar	1050	Sherg 6	Glass, pyrox, mgnt, ilm	Re loop

Sh6-1050-FMQ-0.5	-0.5	96 hrs	1 bar	1050	Sherg 6	Glass, pyrox, mgnt, ilm	Re loop
Sh6-1050-FMQ	0	96 hrs	1 bar	1050	Sherg 6	Glass, pyrox	Re loop
Sh6-1050-FMQ+0.5	+0.5	96 hrs	1 bar	1050	Sherg 6	Glass, pyrox	Re loop
Sh1-1100-FMQ-1	-1	96 hrs	1 bar	1100	Sherg 1	Glass, phos, pyrox	Re loop
Sh1-1050-FMQ-1	-1	96 hrs	1 bar	1050	Sherg 1	Glass, phos, pyrox	Re loop
Sh1-1000-FMQ-1	-1	96 hrs	1 bar	1000	Sherg 1	Glass, mgnt, pyrox, phos	Re loop
Sh6-1000-FMQ-1	-1	168 hrs	1 bar	1000	Sherg 1	Glass, mgnt, pyrox, phos	Re loop
21 [b]	-2.5	2 hrs	0.8 GPa	1300	Sherg 1	Glass	graphite
20 [b]	-2.5	6 hrs	0.8 GPa	1300	Sherg 1	Glass	graphite
16 [b]	-2.5	5 hrs	0.8 GPa	1350	Sherg 1	Glass	graphite
13 [b]	-2.5	4 hrs	0.8 GPa	1400	Sherg 1	Glass	graphite
6 [b]	-2.5	2 hrs	0.8 GPa	1450	Sherg 1	Glass	graphite
29 [b]	-2.5	1 hrs	0.8 GPa	1500	Sherg 1	Glass	graphite
ShR-1	-3.0	3 hrs	1 GPa	1400	Sherg 1	Glass	Mo
ShR-2c	-2.5	3 hrs	1.5	1400	Sherg 1	Glass	graphite
ShR-2b	-3.0	3 hrs	1.5	1400	Sherg 1	Glass	Mo
612	-2.5	3 hrs	2.0	1500	Sherg 1	Glass	graphite
ShR-4a	-3.0	2 hrs	3.0	1500	Sherg 1	Glass	Mo
ShR-4b	-2.5	2 hrs	3.0	1500	Sherg 1	Glass	graphite
BJJB-187	-3.0	22 min	4.0	1600	Sherg 1	Glass	Mo
BJJB-188	-2.5	20 min	4.0	1600	Sherg 1	Glass	graphite
BJJB-189	-2.5	20 min	4.0	1600	Sherg 1	Glass	graphite

724 a- Experiments from McCoy and Lofgren (1999)
725 b- Experiments from Righter et al. (2009)
726 c- Experiments from Morris et al. (2008a)
727 d- ΔFMQ is fO2 relative to the fayalite-magnetite-quartz buffer of O'Neill et al. (1987).

728

729 **Table 3:** Analyses of experimental glasses ($Fe^{3+}/\Sigma Fe$ determined by Mössbauer for 1 bar glasses and XANES for all others)

	capsule	T	P	ΔFMQ	logfO_2	SiO_2	TiO_2	Al_2O_3	FeO	MnO	MgO	CaO	Na_2O	K_2O	P_2O_5	$Fe^{3+}/\Sigma Fe$	Total
FMQ+3	Re loop	1250	1 bar	3	-4.76	55.33	1.3	4.27	19.3	0.26	5.05	10.34	1.81	0.26	0.36	0.28	98.27
FMQ+2	"	1250	1 bar	2	-5.76	55.76	1.27	4.48	19.2	0.24	5.17	10.33	1.76	0.26	0.37	0.21	98.82
FMQ+1	"	1250	1 bar	1	-6.76	55.15	1.24	4.56	19.8	0.26	4.87	10.23	1.82	0.26	0.36	0.13	98.58
FMQ 0.69 P2O5	"	1250	1 bar	0	-7.76	55.99	1.2	4.5	19.5	0.38	4.83	10.34	1.7	0.27	0.31	0.07	99.00
FMQ 1.0 P2O5	"	1250	1 bar	0	-7.76	54.43	1.29	5.17	19.2	0.32	5.37	10.97	1.61	0.37	0.02	0.06	98.79
FMQ 1.5 P2O5	"	1250	1 bar	0	-7.76	54.22	1.22	4.96	19.3	0.42	4.96	11.09	1.41	0.33	1.4	0.07	99.30
FMQ 3.0 P2O5	"	1250	1 bar	0	-7.76	51.65	1.46	5.03	20.4	0.41	5.23	10.62	1.33	0.2	2.71	0.05	98.99
FMQ-1	"	1250	1 bar	-1	-8.76	55.81	1.25	4.88	18.7	0.34	5.15	10.46	1.69	0.24	0.38	0.03	98.86
FMQ-2	"	1250	1 bar	-2	-9.76	57.52	1.24	4.91	17.1	0.32	5.39	10.69	1.67	0.25	0.4	0.02	99.52
FMQ-3	"	1250	1 bar	-3	-10.76	58.13	1.46	4.76	15.8	0.37	5.39	11.15	1.56	0.26	0.29	0.03	99.20
ShR-2c	C	1400	1.5 GPa	-2.5	-8.37	54.12	1.37	4.77	18.7	0.25	5.61	10.1	1.79	0.25	0.39	0.06	97.39
612	C	1500	2 GPa	-2.5	-7.43	53.06	1.48	3.83	22.1	0.28	3.26	10.98	2.21	0.34	0.48	0.07	98.03
ShR-4b	C	1500	3 GPa	-2.5	-7.15	53.60	1.24	4.56	18.9	0.3	7.11	9.4	1.69	0.25	0.39	0.06	97.233
188	C	1600	4 GPa	-2.5	-6.19	46.51	0.73	3.83	10.8	0.11	25.77	11.03	1.11	0.15	0.53	0.03	100.59
6	C	1450	0.8 GPa	-2.5	-8.16	52.4	0.76	4.6	17.7	0.2	10.2	10.76	1.48	0.3	0.63	0.02	99.03
13	C	1400	0.8 GPa	-2.5	-8.58	51.1	0.61	4.6	15.1	0.21	12.4	11.84	1.11	0.13	0.61	0.03	97.70
16	C	1350	0.8 GPa	-2.5	-9.02	53	0.78	5.8	14	0.22	11.8	11	1.16	0.19	0.63	0.02	98.57
20	C	1300	0.8 GPa	-2.5	-9.49	45.3	1.44	8.1	27.8	0.36	3.1	8.36	2.34	0.46	1.11	0.02	98.34
21	C	1300	0.8 GPa	-2.5	-9.49	49.5	0.66	7.6	18.1	0.34	9.2	11.78	1.18	0.2	0.64	0.02	99.17
29	C	1500	0.8 GPa	-2.5	-7.77	54.9	1.78	6.02	17.2	0.17	6.31	9.08	1.63	0.41	0.77	0.04	98.30
189	C	1600	4 GPa	-2.5	-6.19	46.75	1	2.93	15.9	0.21	18.1	10.92	1.49	0.2	0.45	0.03	97.98
ShR-1	Mo	1400	1 GPa	-3	-9.02	53.51	0.98	3.42	16.9	0.13	5.8	12.81	2.7	0.39	0.21	0.16	97.01
ShR-2b	Mo	1400	1.5 GPa	-3	-8.87	53.10	1.02	3.48	21	0.31	5.49	10.09	1.87	0.25	0.41	0.07	97.02
ShR-4a1	Mo	1500	3 GPa	-3	-7.65	53.42	0.91	4.36	20.2	0.22	6.2	9.52	1.81	0.24	0.36	0.12	97.27
187	Mo	1600	4 GPa	-3	-6.69	53.59	0.94	5.43	18.9	0.34	4.83	9.74	1.79	0.26	0.41	0.05	96.19

730

731 **Table 4: Subliquidus magnetite stability experiment phases**

	phase	SiO_2	TiO_2	Al_2O_3	Fe_2O_3	FeO	MnO	MgO	CaO	Na_2O	K_2O	P_2O_5	Total
FMQ-1, sherg1	gl	57.7	1.06	6.94	-	18.66	0.25	3.65	8.90	1.17	0.38	0.59	99.30
1000 C	px	49.28	0.60	0.61	-	26.84	0.43	8.40	12.40	0.14	0.01	0	98.72
	Mgnt #	0.43	25.97	1.73	-	65.69	0.34	0.72	0.28	0	0.02	0	95.20
					11.82	55.05							96.34
FMQ-1, sherg1	gl	54.6	1.76	5.68	-	19.84	0.27	4.64	10.08	1.52	0.33	0.48	99.20
1050 C	px	50.38	0.59	0.61	-	22.69	0.46	9.31	15.34	0.23	0	0.05	99.66
	qtz	98.87	0.12	0.65	-	0.64	0.01	0.08	0.20	0.25	0.02	0	100.84
FMQ+0.5, sherg1	gl	57.07	1.85	7.59	-	20.86	0.26	1.59	7.33	2.35	0.47	0.67	100.03
1050 C	px	50.61	0.46	0.58	-	21.0	0.39	9.98	16.36	0.26	0.00	0.06	99.70
	qtz	97.67	0.22	2.06	-	0.48	0	0	0.12	0.64	0.01	0.03	101.24
FMQ-0.5, sherg1	gl	56.2	1.78	6.52	-	19.89	0.26	2.35	8.35	2.12	0.40	0.55	98.42
1050 C	px	50.76	0.64	0.48	-	23.06	0.43	9.02	15.64	0.16	0	0.03	100.21
ZAG 063	gl *	48.8	1.12	8.66	-	19.8	0.52	5.60	9.95	2.01	0.19	0.85	97.47
ZAG 064	gl *	59.9	1.07	9.58	-	9.48	0.43	4.95	8.23	2.31	0.26	1.08	97.29
	Mgnt#	0.88	1.09	2.43	-	81.25	0.75	6.56	0.23	-	-	-	93.23
					32.60	54.07							99.50

732

733 *Analysis from McCoy and Lofgren (1999)

734 # totals for magnetite are low due to presence of some Fe_2O_3 ; analyses were recalculated according to charge balance and stoichiometry and
735 adjusted totals are shown on the line below each magnetite analysis.

736

737

Table 5. P_2O_5 concentrations, Mössbauer parameters[a], and $Fe^{3+}/\Sigma Fe$ ratio for shergottite composition glasses.

		Fe^{2+} Doublet				Fe^{2+} Doublet				Fe^{3+} Doublet				
	P_2O_5 (wt.%)	δ (mm/s)	ΔE_Q (mm/s)	FWHM (mm/s)	A (%)	δ (mm/s)	ΔE_Q (mm/s)	FWHM (mm/s)	A (%)	δ (mm/s)	ΔE_Q (mm/s)	FWHM (mm/s)	A (%)	$Fe^{3+}/\Sigma Fe$
Sherg1, FMQ+3	0.7	1.05	2.11	0.51	45	0.99	1.56	0.51	27	0.34	1.15	0.65	28	0.28
Sherg1, FMQ+2	0.7	1.06	2.17	0.47	44	1.00	1.60	0.47	36	[0.34][b]	[1.15]	[0.65]	20	0.20
Sherg1, FMQ+1	0.7	1.06	2.14	0.49	49	1.00	1.58	0.48	38	[0.34]	[1.15]	[0.65]	13	0.13
Sherg1, FMQ	0.7	1.06	2.15	0.50	51	1.00	1.58	0.50	42	[0.34]	[1.15]	[0.65]	7	0.07
Sherg1a, FMQ	1.0	1.06	2.18	0.50	53	1.00	1.61	0.50	41	[0.34]	[1.15]	[0.65]	6	0.06
Sherg1b, FMQ	1.5	1.06	2.19	0.51	50	1.00	1.60	0.51	43	[0.34]	[1.15]	[0.65]	7	0.07
Sherg1c FMQ	3.0	1.05	2.15	0.50	54	0.99	1.56	0.50	41	[0.34]	[1.15]	[0.65]	5	0.05
Sherg1, FMQ-1	0.7	1.06	2.15	0.50	55	1.00	1.55	0.50	42	[0.34]	[1.15]	[0.65]	3	0.03
Sherg1, FMQ-2	0.7	1.06	2.14	0.49	54	0.99	1.56	0.49	44	[0.34]	[1.15]	[0.65]	2	0.02
Sherg1, FMQ-3	0.7	1.05	2.12	0.50	57	0.99	1.53	0.50	40	[0.34]	[1.15]	[0.65]	3	0.03
ZAG 053, FMQ	---	1.06	2.18	0.50	55	1.00	1.52	0.50	43	[0.34]	[1.15]	[0.65]	3	0.02
Uncertainty[c]	---	±0.02	±0.02	±0.02	±2	±0.02	±0.02	±0.02	±2	±0.02	±0.02	±0.02	±2	±0.02

[a]Mössbauer parameters: δ = center shift referenced to the midpoint of the spectrum of metallic iron foil at room temperature; ΔE_Q = quadrupole splitting; FWHM = full width at half maximum intensity; A = subspectral area (*f*-factor corrected).

[b]Parameters in square brackets are initial values and were constrained to those values during the least-squares fitting procedure. The values δ, ΔE_Q, and FWHM for the Fe^{3+} doublet subspectrum were calculated from the spectrum for Sherg1 (FMQ+3)), and those values were used as fitting constraints for the other

spectra.

[c]Uncertainty for non-constrained parameters.

738

739 **Table 6: XANES data for experimental glasses**

Sample	Area 1	Center 1	Area 2	Center 2	centroid	$Fe^{3+}/\Sigma Fe$
ZAG-064	0.1089	7.112790	0.4365	7.114280	7.113982	0.80
ZAG-063	0.3944	7.112430	0.2487	7.114000	7.113037	0.15
sh1-1000-FMQ-1	0.2677	7.112300	0.1192	7.113690	7.112728	0.03
sh1-1050-FMQ	0.4104	7.112400	0.2073	7.113820	7.112876	0.08
sh1-1050-FMW+0.5	0.4636	7.112370	0.1731	7.113720	7.112737	0.03
sh6-1050-FMQ-0.5	0.2211	7.112380	0.0692	7.113540	7.112656	0.01
6	0.2996	7.112350	0.1088	7.113660	7.112699	0.02
13	0.3715	7.112390	0.1236	7.113720	7.112722	0.03
16	0.4384	7.112370	0.1490	7.113670	7.112700	0.02
20	0.44	7.1124	0.1490	7.113670	7.112700	0.02
21	0.2954	7.112390	0.0942	7.113680	7.112702	0.02
29	0.2825	7.112410	0.0997	7.113790	7.112770	0.04
612	0.6256	7.112460	0.2432	7.113860	7.112852	0.07
ShR-1	0.3078	7.112490	0.1687	7.114080	7.113053	0.16
ShR-2B	0.3096	7.112470	0.1175	7.113870	7.112855	0.07
ShR-2C	0.4346	7.112430	0.1659	7.113820	7.112814	0.06
ShR-4A	0.3275	7.112490	0.1503	7.114030	7.112975	0.12
ShR-4B	0.3709	7.112340	0.1685	7.113860	7.112815	0.06
BJJB-187	0.2557	7.112400	0.0972	7.113790	7.112783	0.05
BJJB-188	0.1307	7.112260	0.0816	7.113960	7.112913	0.10
BJJB-189	0.2995	7.112330	0.1196	7.113730	7.112730	0.03

740

741

742 **Table 7: Fit parameters for equation (2); *n* = 22, *r* = 0.931; std. err = 0.41**

Constant	value	error
a ($lnfO_2$)	0.22	0.039
b (1/T)	3800	580
c (P/T)	-370	35
d (X_{FeO})	-6.6	1.7
e (X_{Al2O3})	7.3	3.1
f (X_{CaO})	17.3	9.8
g (X_{Na2O})	132.3	25.8
h (X_{K2O})	-147.8	32.5
i (X_{P2O5})	0.60	0.21
j (constant)	-4.26	0.55

743

744

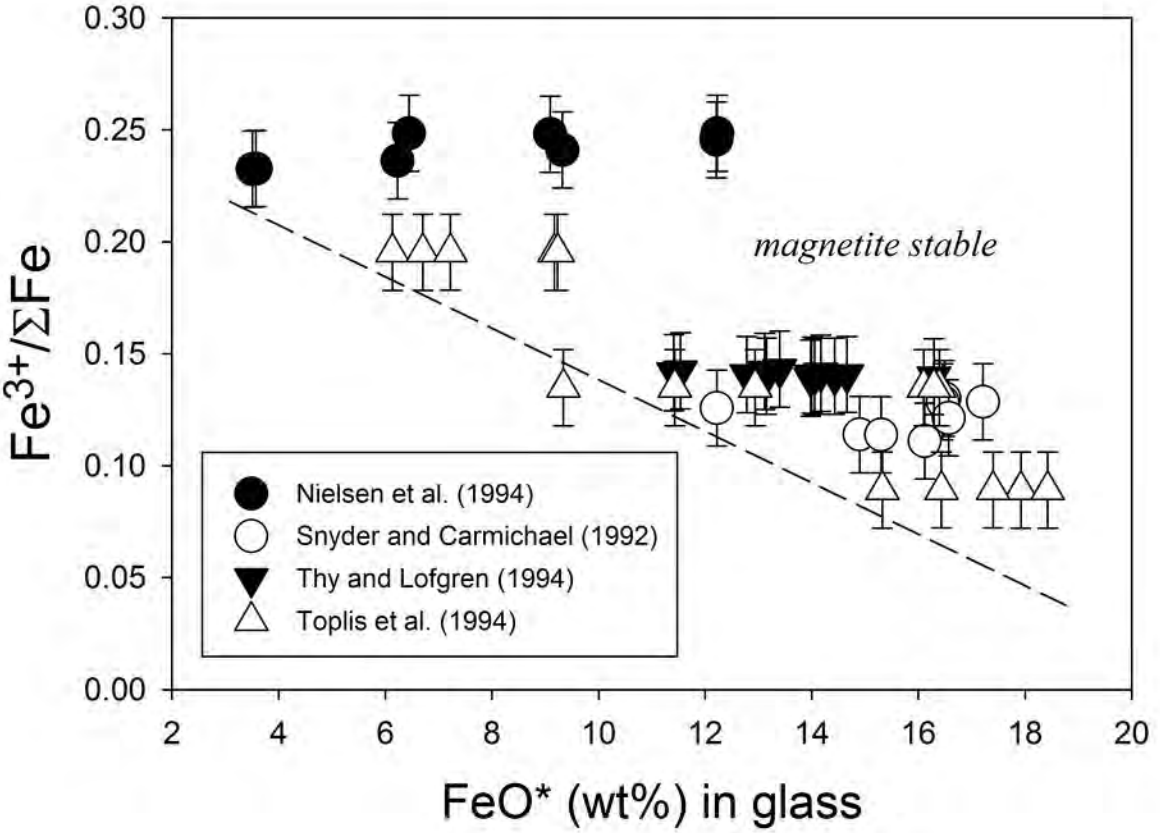
0.30
0.25
0.20
0.15
0.10
0.05
0.00
Fe3+/ΣFe
2
4
6
8
10
12
14
16
18
20
FeO* (wt%) in glass
magnetite stable
Nielsen et al. (1994)
Snyder and Carmichael (1992)
Thy and Lofgren (1994)
Toplis et al. (1994)

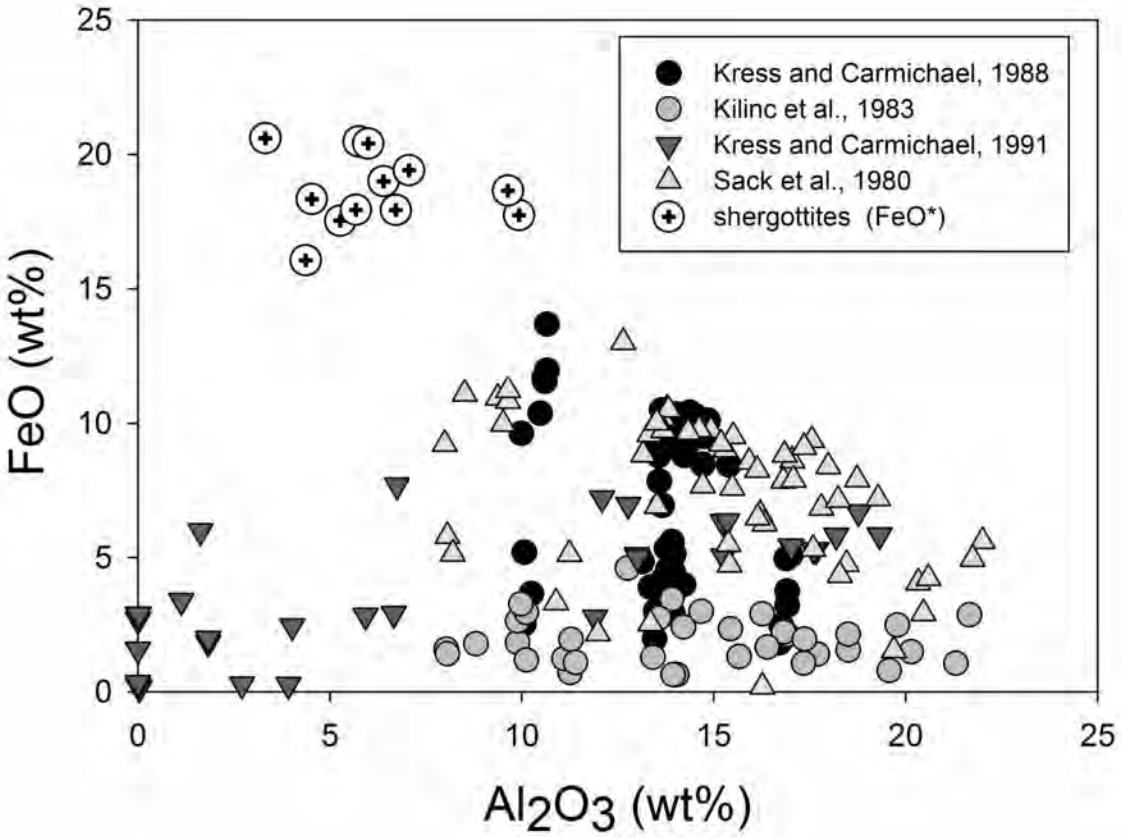
Kress and Carmichael, 1988
Kilinc et al., 1983
Kress and Carmichael, 1991
Sack et al., 1980
shergottites (FeO*)
FeO (wt%)
Al2O3 (wt%)
0
5
10
15
20
25

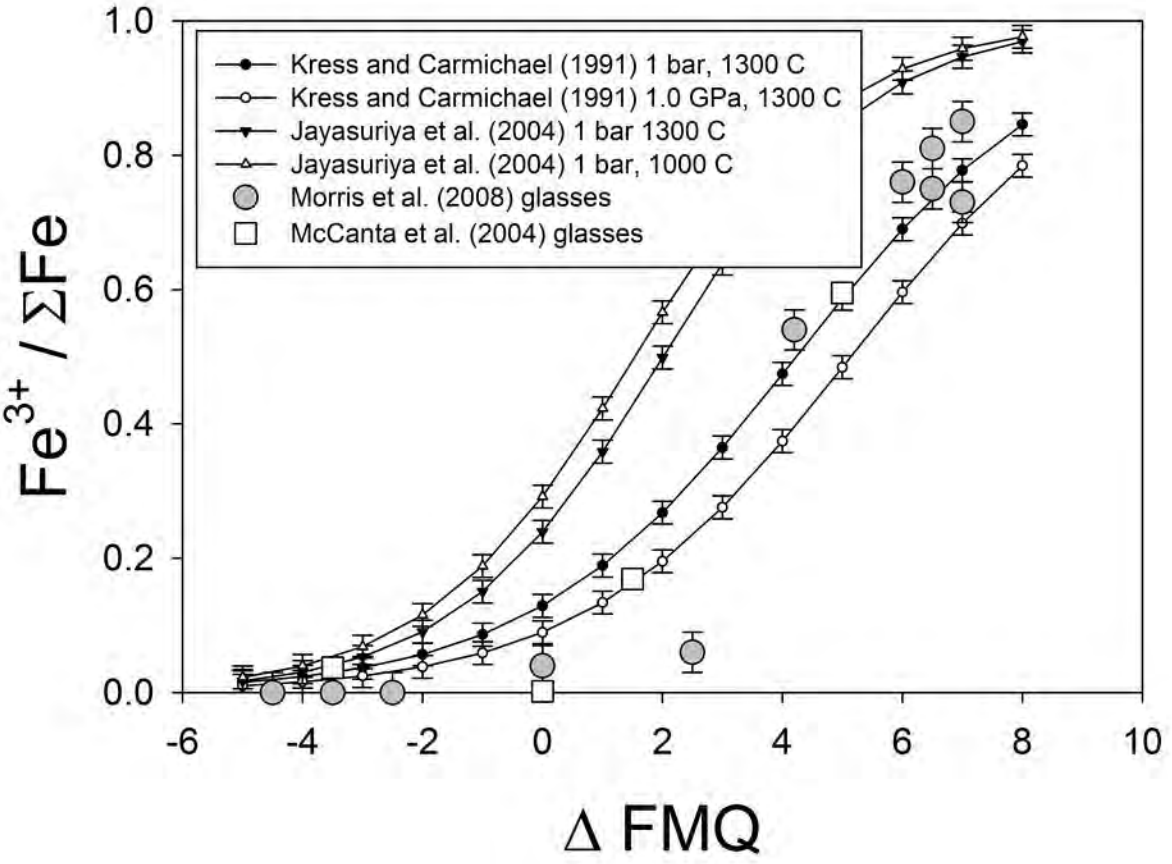
Kress and Carmichael (1991) 1 bar, 1300 C
Kress and Carmichael (1991) 1.0 GPa, 1300 C
Jayasuriya et al. (2004) 1 bar 1300 C
Jayasuriya et al. (2004) 1 bar, 1000 C
Morris et al. (2008) glasses
McCanta et al. (2004) glasses
Fe3+ / ΣFe
Δ FMQ
1.0
0.8
0.6
0.4
0.2
0.0
-6
-4
-2
0
2
4
6
8
10

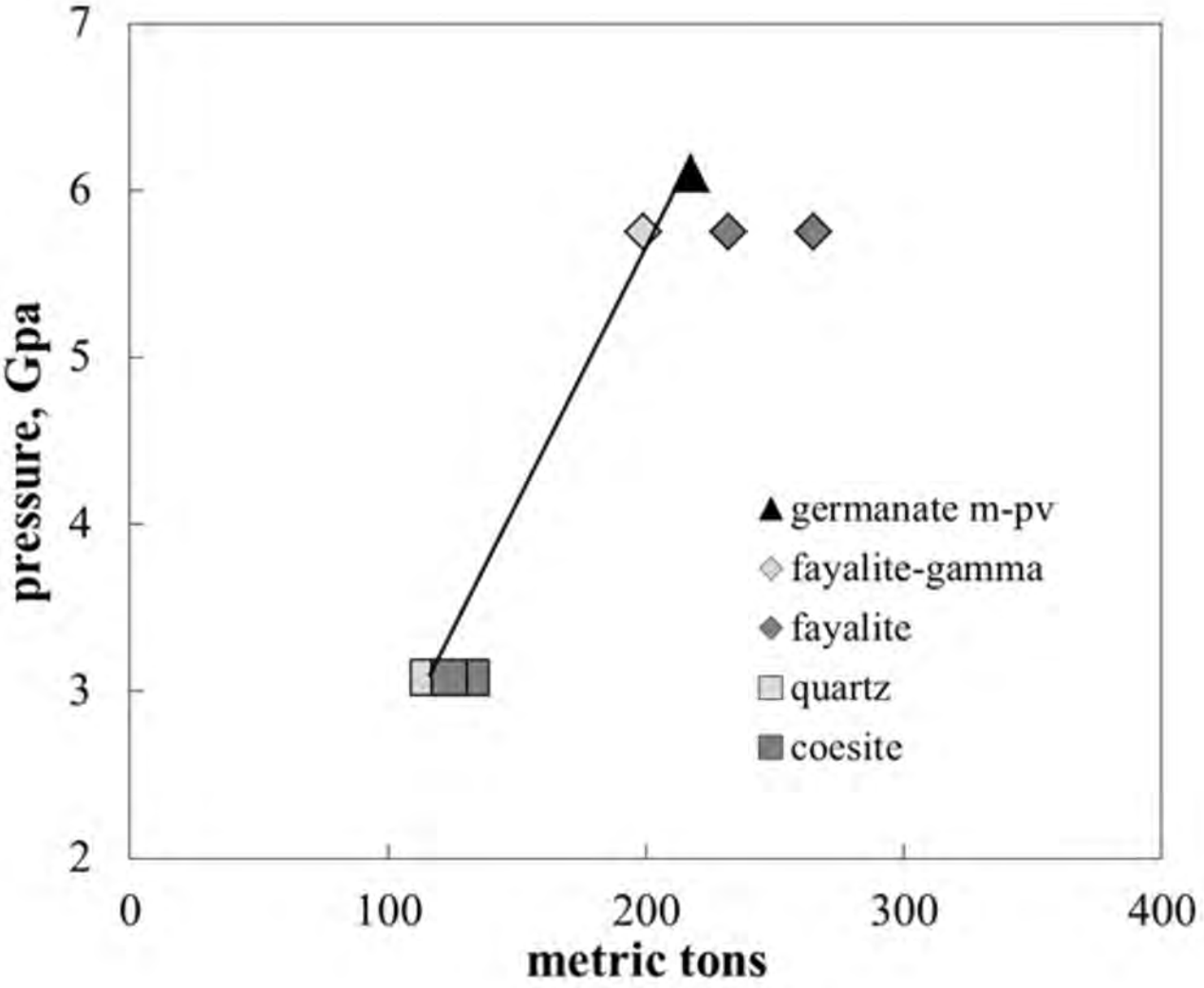
7
6
5
4
3
2
pressure, Gpa
0
100
200
300
400
metric tons
germanate m-pv
fayalite-gamma
fayalite
quartz
coesite

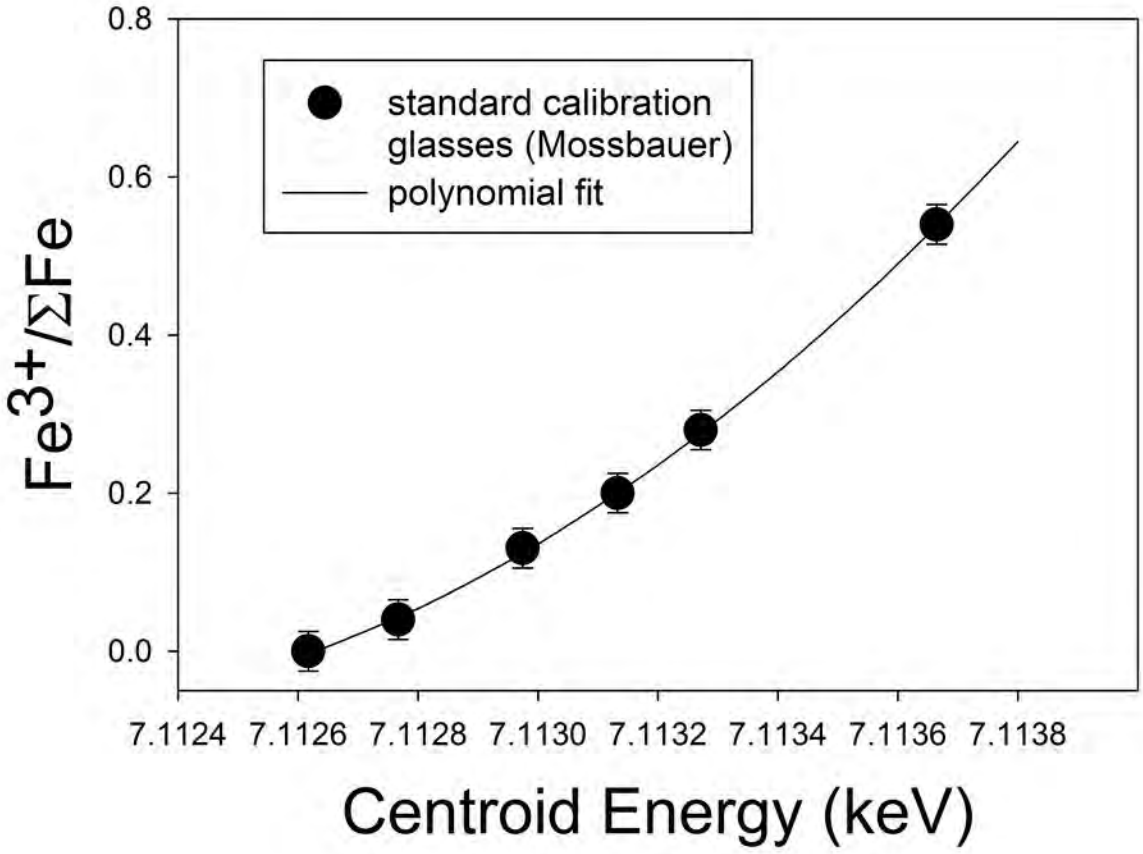
0.8
0.6
0.4
0.2
0.0
Fe3+/ΣFe
standard calibration
glasses (Mossbauer)
polynomial fit
7.1124
7.1126
7.1128
7.1130
7.1132
7.1134
7.1136
7.1138
Centroid Energy (keV)

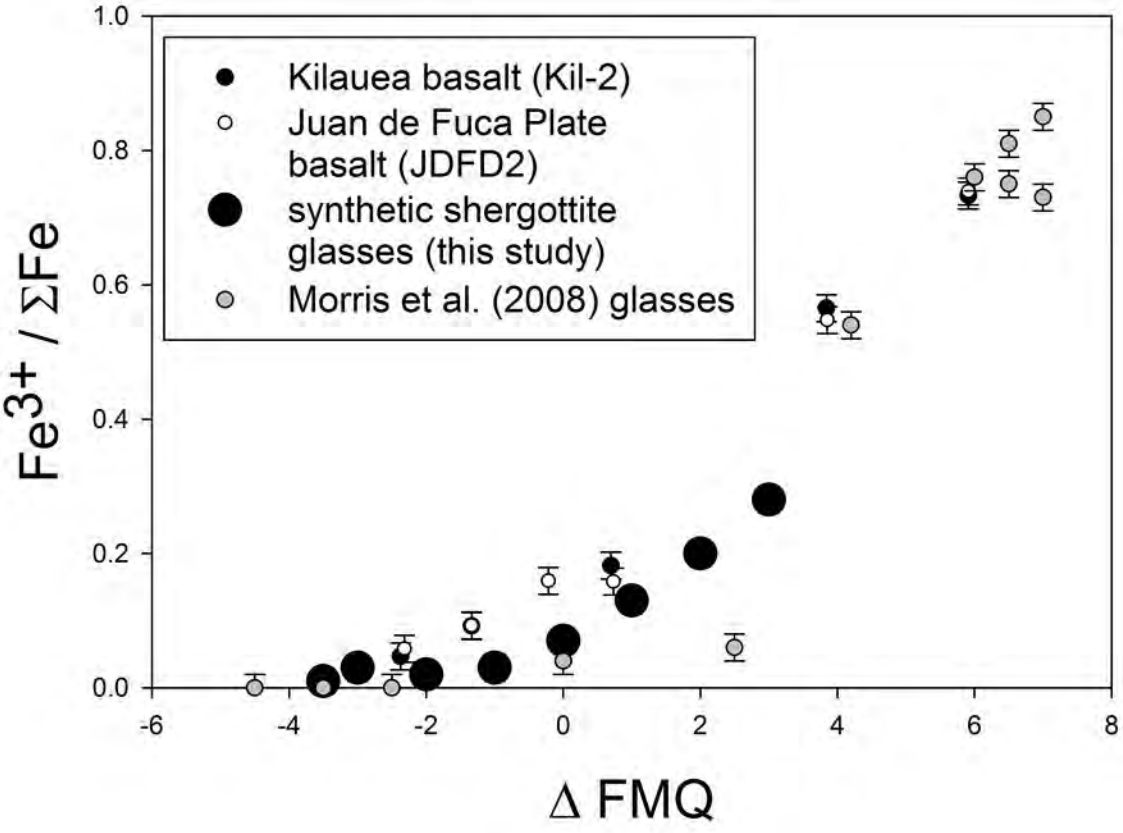
Kilauea basalt (Kil-2)
Juan de Fuca Plate basalt (JDFD2)
synthetic shergottite glasses (this study)
Morris et al. (2008) glasses
Fe3+ / ΣFe
Δ FMQ
1.0
0.8
0.6
0.4
0.2
0.0
-6
-4
-2
0
2
4
6
8

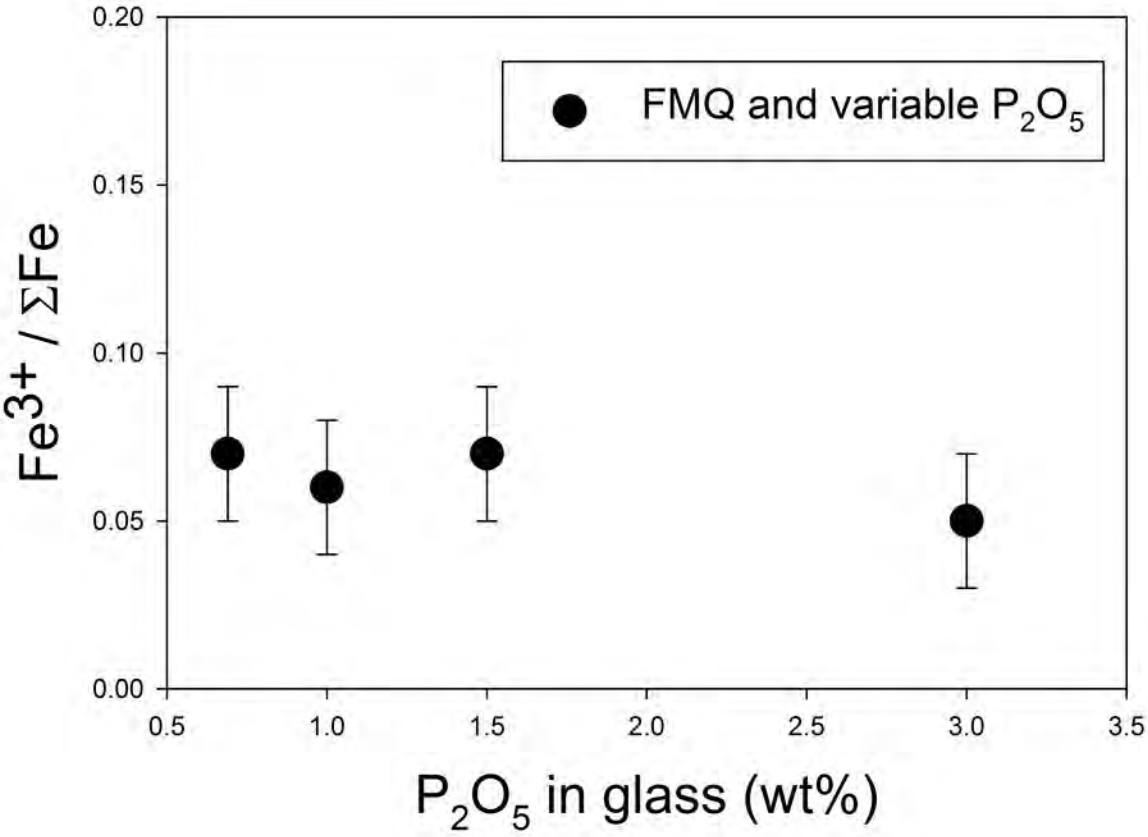
0.20
0.15
0.10
0.05
0.00
0.5
1.0
1.5
2.0
2.5
3.0
3.5
FMQ and variable P2O5
Fe3+ / ΣFe
P2O5 in glass (wt%)

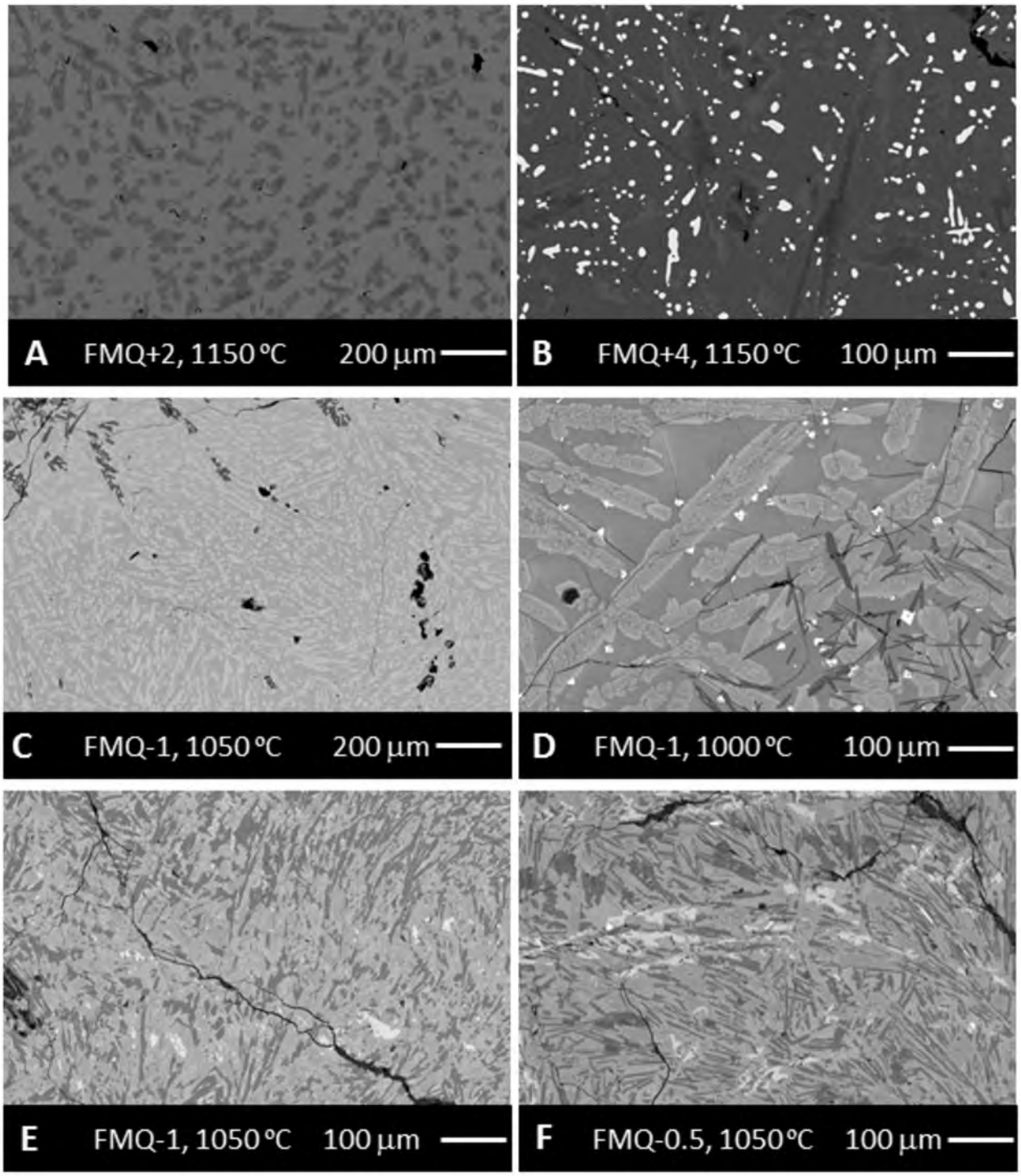
A FMQ+2, 1150 °C 200 µm
B FMQ+4, 1150 °C 100 µm
C FMQ-1, 1050 °C 200 µm
D FMQ-1, 1000 °C 100 µm
E FMQ-1, 1050 °C 100 µm
F FMQ-0.5, 1050 °C 100 µm

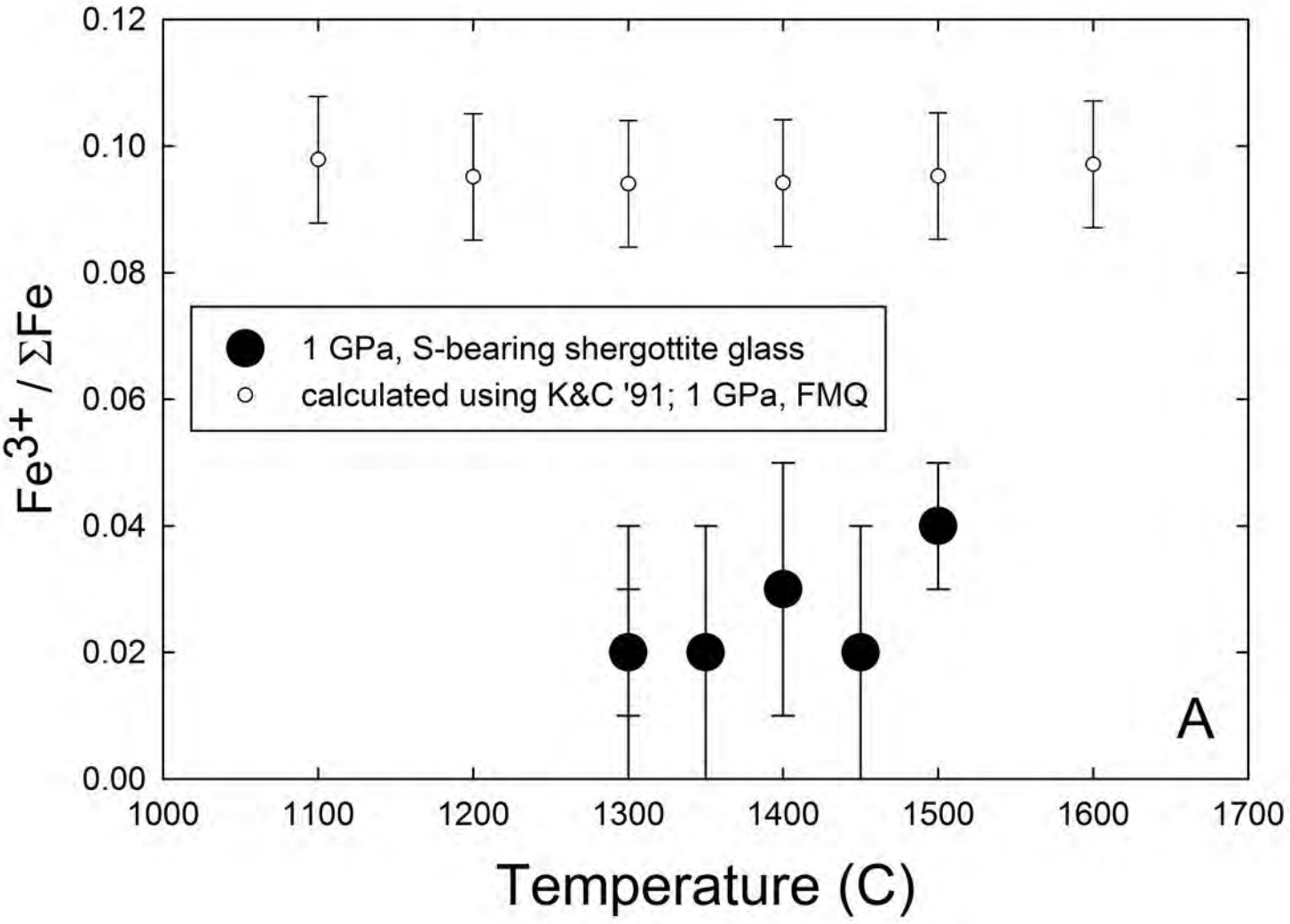
0.12
0.10
0.08
0.06
0.04
0.02
0.00
Fe3+ / ΣFe
1 GPa, S-bearing shergottite glass
calculated using K&C '91; 1 GPa, FMQ
A
1000
1100
1200
1300
1400
1500
1600
1700
Temperature (C)

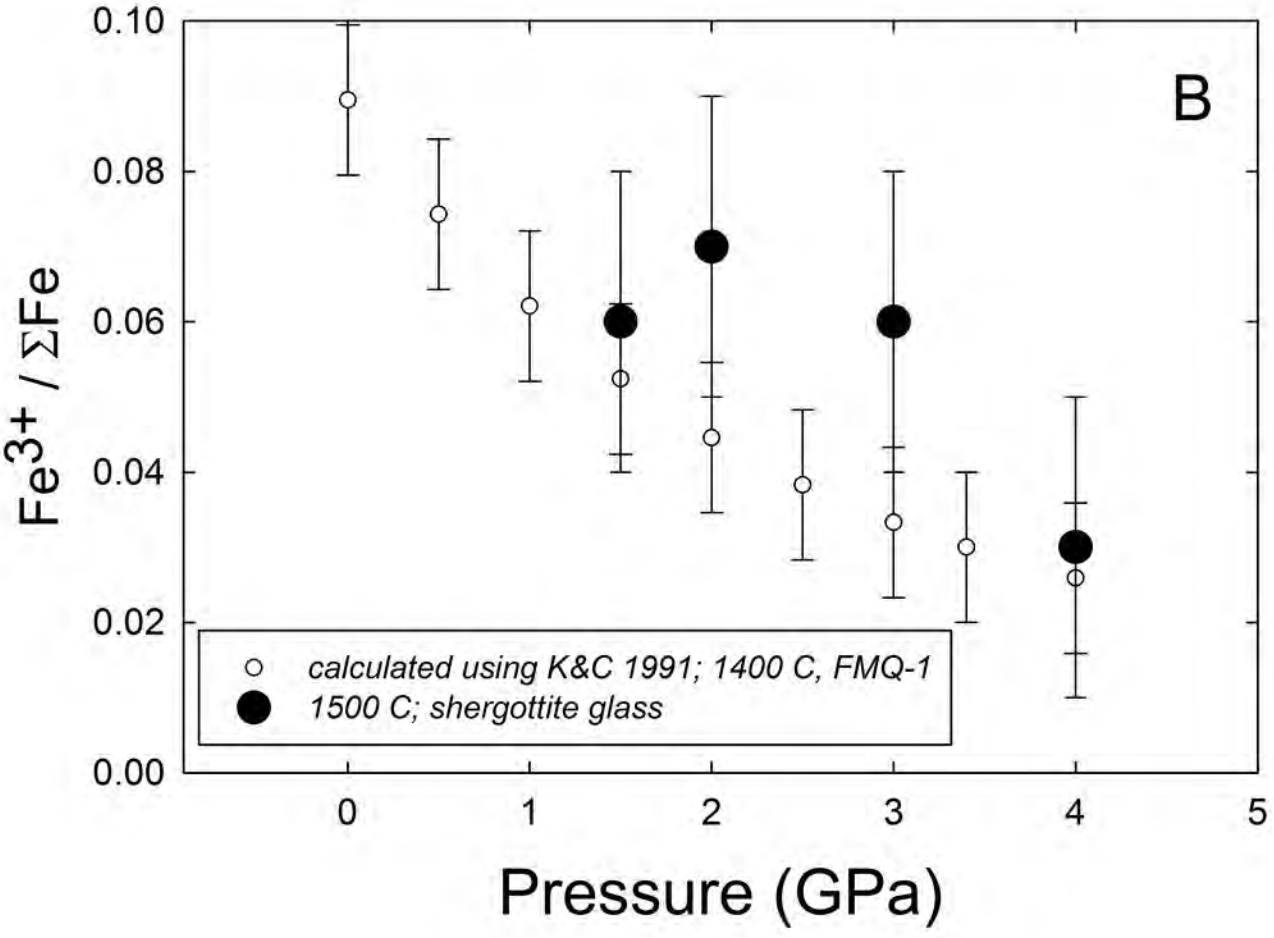
B
0.10
0.08
0.06
0.04
0.02
0.00
Fe^{3+} / ΣFe
0
1
2
3
4
5
Pressure (GPa)
calculated using K&C 1991; 1400 C, FMQ-1
1500 C; shergottite glass

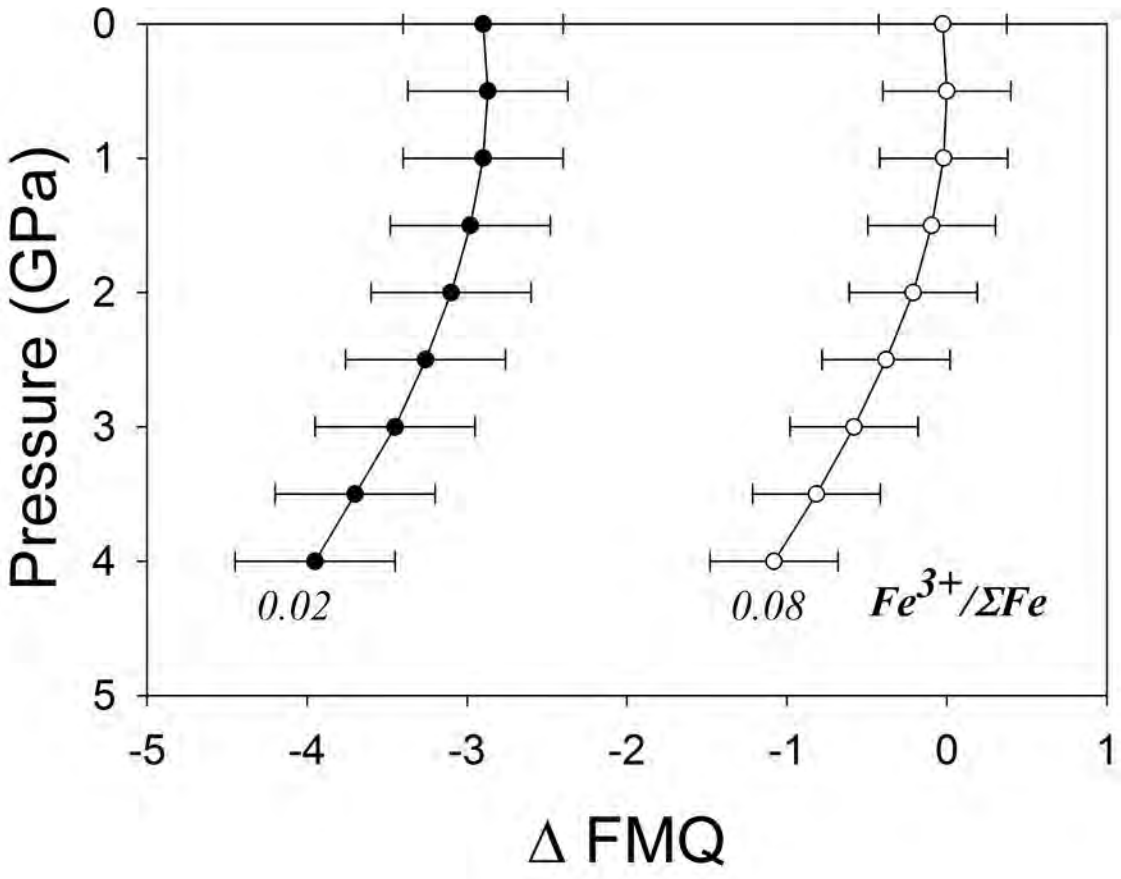
Pressure (GPa)
0
1
2
3
4
5
-5
-4
-3
-2
-1
0
1
Δ FMQ
0.02
0.08
Fe3+/ΣFe

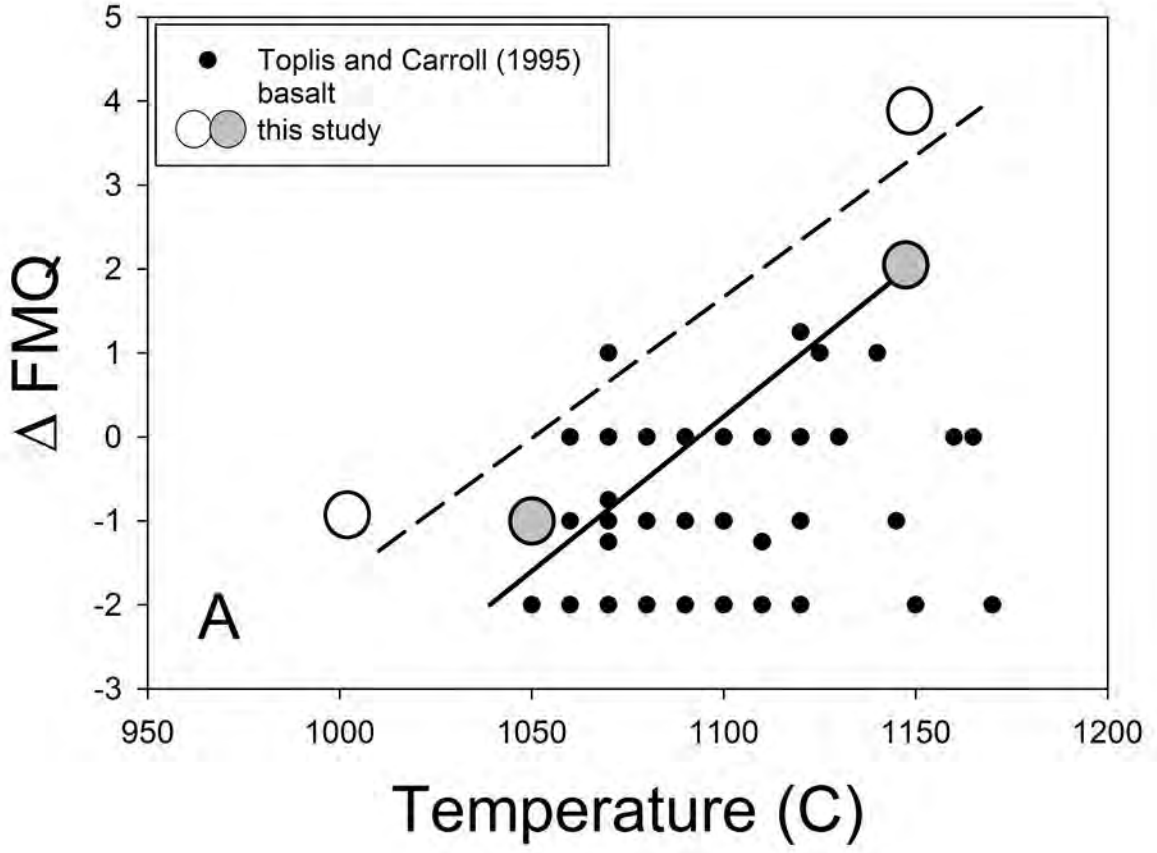
Toplis and Carroll (1995)
basalt
this study
A
Δ FMQ
Temperature (C)
5
4
3
2
1
0
-1
-2
-3
950
1000
1050
1100
1150
1200

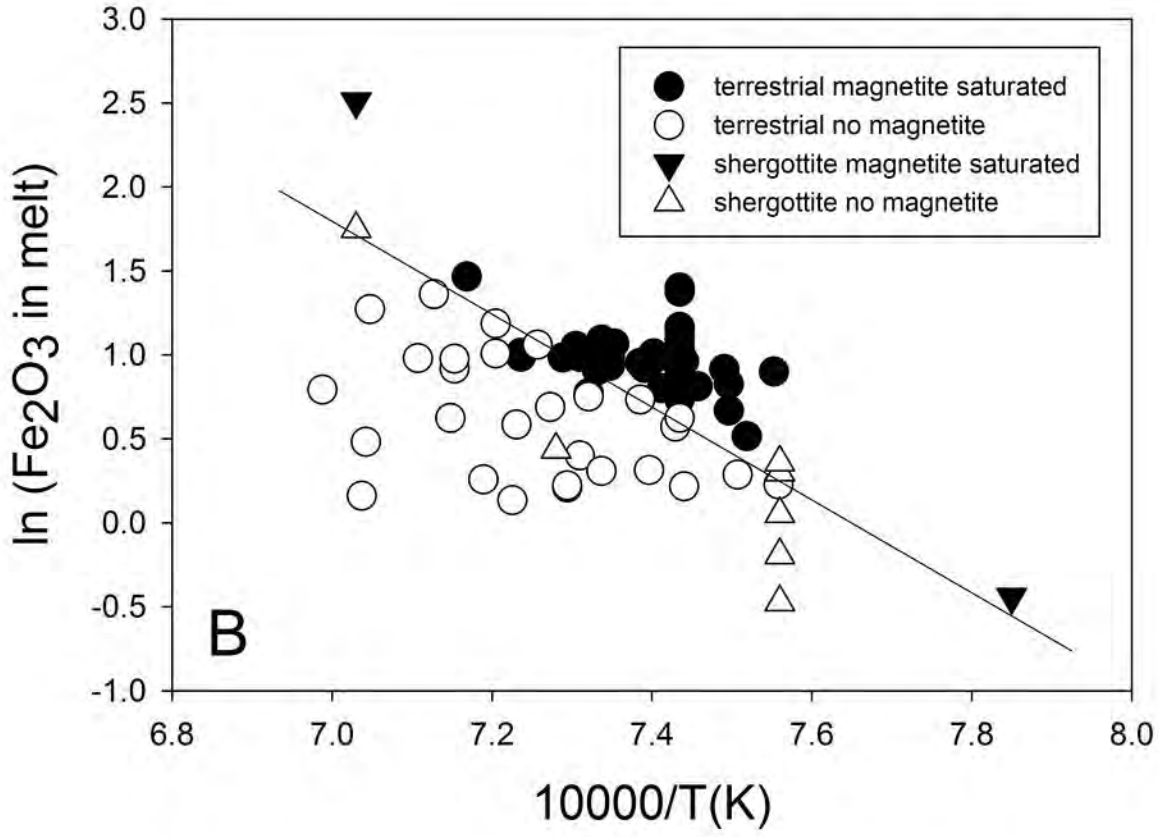
terrestrial magnetite saturated
terrestrial no magnetite
shergottite magnetite saturated
shergottite no magnetite
B
ln (Fe2O3 in melt)
10000/T(K)
3.0
2.5
2.0
1.5
1.0
0.5
0.0
-0.5
-1.0
6.8
7.0
7.2
7.4
7.6
7.8
8.0

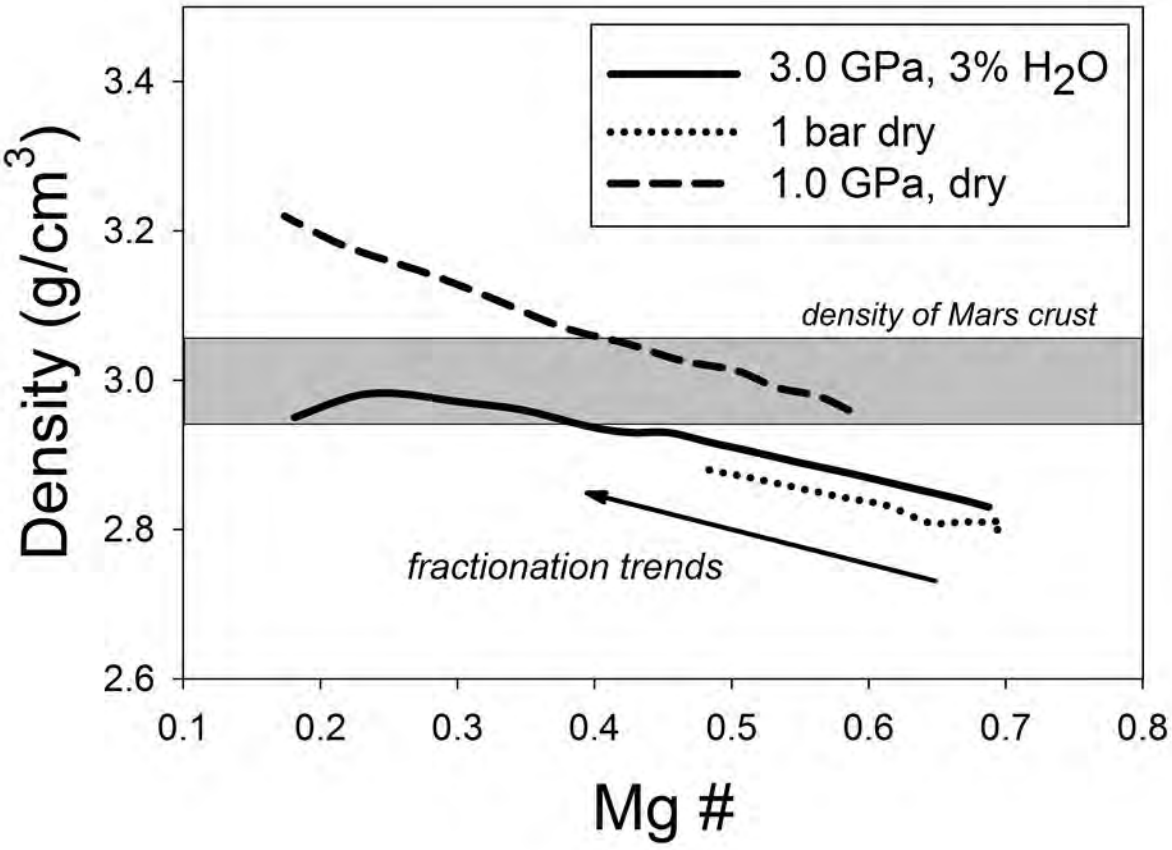
3.0 GPa, 3% H2O
1 bar dry
1.0 GPa, dry
density of Mars crust
fractionation trends
Density (g/cm3)
Mg #
3.4
3.2
3.0
2.8
2.6
0.1
0.2
0.3
0.4
0.5
0.6
0.7
0.8